CHAPTER

Microfluidics and micro total analytical systems

3

CHAPTER OUTLINE

3.1 INTRODUCTION

Microfluidics is an emerging field that studies the behavior and control of fluids that are constrained geometrically to small scales. It is an enabling technology to perform biological and chemical experiments at greatly reduced spatial scales, with minimal material consumption and high-throughput. It is based on the control of flows in microchannels with characteristic dimensions ranging from millimeters to micrometers, constituting the basis of technologies known as micro total analysis systems (μTAS) or labs-on-a-chip (LOC).

Microfluidics allows for handling of fluid with volumes typically in the range of nano- to microliters (10^{-9} to 10^{-6} L) or smaller. Microfluidics is key to advancing molecular sensors based on bioassays including immunoassay, cell separation, DNA amplification, and analysis, among many other examples. Microfluidic systems process a large number of parallel experiments rapidly with a small amount of reagent and automate chemical, biological, and medical applications on a large scale with low cost. For example, reducing the reaction chamber size by a factor of 10 increases the reaction rate by a factor of 100 because the smaller characteristic length of the system decreases diffusion time. In addition to faster reaction times, the amounts of analyte and reagents required are also reduced proportionally to the reduction of the reaction chamber volume. Not only does this reduce the cost of the test by reducing

Molecular Sensors and Nanodevices. https://doi.org/10.1016/B978-0-12-814862-4.00003-X

the required amounts of chemicals, it also allows more types of tests to be conducted in parallel with the same size of sample.

In this chapter, we first discuss basic theories of fluid dynamics that are essential to characterize microfluidic systems: diffusion and the laminar flow. Fick's laws of diffusion and the solutions to simple cases of incompressible laminar flows are explained. Two important dimensionless numbers, Reynolds number and Péclet number, are discussed to characterize flows and diffusion in microchannels.

We then introduce examples of microfluidic μTAS or LOC elements and systems that are important to molecular sensing. Examples of basic microfluidic components include microfluidic mixers and sorters for molecular analysis, where molecules and reagent solutions are manipulated and studied through multiple micro channels and chambers. Applications of microfluidic systems in the biomedical and molecular analysis include particle separators and cell sorters for microfluidic cellular analysis. We also describe methods of genomic analysis including DNA/RNA amplification, serration, and sequencing.

3.2 MICROFLUIDICS FUNDAMENTALS

3.2.1 DIFFUSION

Fick's first law of diffusion states that the rate of transfer of molecules from regions of high concentration to regions of low concentration is proportional to the concentration gradient (see Fig. 3.1). In a one-dimensional model of diffusion, the law is expressed as:

$$J = -D\frac{\partial \varphi}{\partial x} \tag{3.1}$$

where J is the flux: number of molecules per unit area per unit time (e.g., mol m^{-2} s^{-1}); D is the diffusion coefficient: length^2 time^{-1} (e.g., m^2/s); and φ is the concentration: number of molecules per unit volume (e.g., mol m^{-3}).

Note the negative sign on the right-hand side of Eq. (3.1). The flux J is positive when the gradient $\frac{\partial \varphi}{\partial x}$ is negative, because diffusion occurs to level the gradient.

Fick's second law can be derived from Fick's first law. Consider a small one-dimensional control volume from x to $x + \Delta x$ with transport only by diffusion

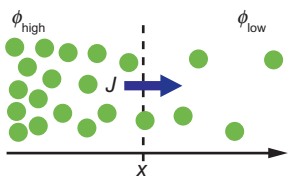

FIG. 3.1

One-dimensional model of diffusion.

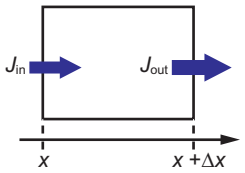

FIG. 3.2

Fick's second law.

(Fig. 3.2). The change in the concentration of molecules with time $\left(=\frac{\partial \varphi}{\partial t}\right)$ is the difference between the flux going in $(=J_{in})$ and the flux going out $(=J_{out})$.

$$\frac{\partial \varphi}{\partial t} = J_{in} - J_{out} \tag{3.2}$$

By using the first law in Eq. (3.1):

$$\frac{\partial \varphi}{\partial t} = -D\left(\left.\frac{\partial \varphi}{\partial x}\right|_{x=x} - \left.\frac{\partial \varphi}{\partial x}\right|_{x=x+\Delta x}\right)/\Delta x \tag{3.3}$$

When Δx approaches zero, Eq. (3.3) becomes:

$$\frac{\partial \varphi}{\partial t} = D\frac{\partial^2 \varphi}{\partial x^2} \tag{3.4}$$

Eq. (3.4) is called *Fick's second law*, or a *diffusion equation*.

A simple but useful case of diffusion is where we consider a semi-infinite region in $x > 0$ with a fixed concentration at the boundary $(\varphi(0,t) = \varphi_0)$, as shown in Fig. 3.3. The solution to this problem is given as:

$$\varphi(x,t) = \varphi_0 \cdot \mathrm{erfc}\left(\frac{x}{2\sqrt{Dt}}\right), \tag{3.5}$$

where erfc is the complementary error function defined as:

$$\mathrm{erfc}(x) = \frac{2}{\sqrt{\pi}}\int_x^\infty e^{-t^2} dt \quad (=1-\mathrm{erf}(x)) \tag{3.6}$$

The graph of $Y =$ erfc (X) is plotted in Fig. 3.4. As one might expect, $\varphi(x,t)$ at a constant position $x = c$ is a monotonically increasing function of time t. It is useful

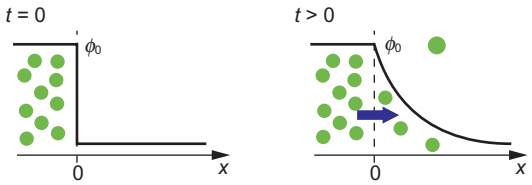

FIG. 3.3

Diffusion from a constant source.

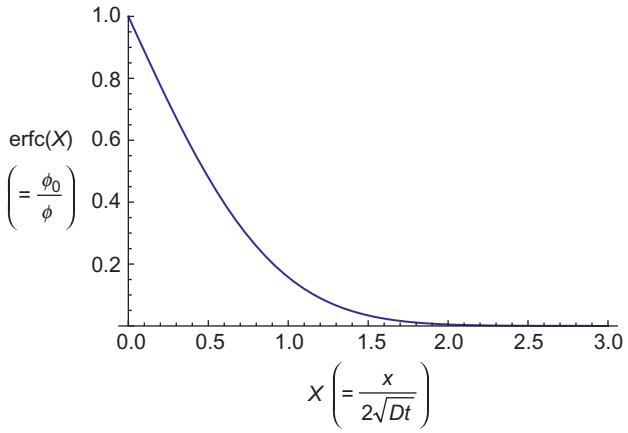

FIG. 3.4

Complementary error function as a solution to the diffusion equation.

to discuss the characteristic diffusion length $L_D = 2\sqrt{Dt}$, where the concentration satisfies $\varphi(\lambda, t) = \varphi_0 \cdot$ erfc (1). As the time t increases, the length λ becomes larger, which means molecules diffuse further.

SUMMARY OF DIFFUSION

Let J, D, φ, t be flux, diffusion coefficient, concentration, and time, respectively.

Fick's first law

$$J = -D\frac{\partial \varphi}{\partial x}$$

Fick's second law

$$\frac{\partial \varphi}{\partial t} = D\frac{\partial^2 \varphi}{\partial x^2}$$

Diffusion length

Diffusion length is proportional to $\sqrt{Dt}$.

3.2.2 LAMINAR FLOW AND HAGEN-POISEUILLE EQUATION

Viscosity

Viscosity quantifies the resistance of a fluid that is being deformed by stress. A simple measurement of viscosity is illustrated with a flow of a viscous fluid in the space between two parallel plates, one of which is moving with a constant velocity U and the other stationary (Fig. 3.5).

In this case, flow velocity u_x in x-direction changes from $u_x = 0$ to $u_x = U$ linearly from $y = 0$ to $y = H$, where H is the distance between the two plates. Such a parallel flow with a constant velocity gradient is called a Couette flow.

Let us define shear stress τ as $\tau = F/A$, where F is the force needed to move the top plate at a velocity U, and A is the area of the plate. Isaac Newton found that the

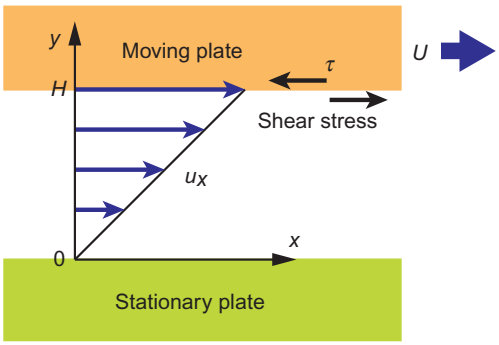

FIG. 3.5

Viscosity in a Couette flow.

shear stress τ is proportional to the velocity gradient U/H for many fluids. The viscosity μ of a fluid is defined as the coefficient of this linear relationship, namely:

$$\tau = \mu \frac{U}{H} \tag{3.7}$$

The term μ is also called the dynamic viscosity. A fluid that satisfies Eq. (3.7) is called a Newtonian fluid.

Next, we discuss a more general case of a flow in a channel, where fluid flows in parallel layers or laminae with no disruption between the layers. Such a flow is called laminar flow. In most cases of microdevices, a flow can be considered laminar (we discuss this issue again with Reynolds number in the next section). The laminar flow can be considered to be layers of thin films (see Fig. 3.6A). The walls are stationary and the fluid is driven by the pressure gradient along the channel. The important assumption is that the flow velocity is continuous at the boundary between the fluid and wall, i.e., the fluid has zero velocity relative to the boundary. This assumption is called the no-slip condition. This condition defines the velocity u_x at the walls.

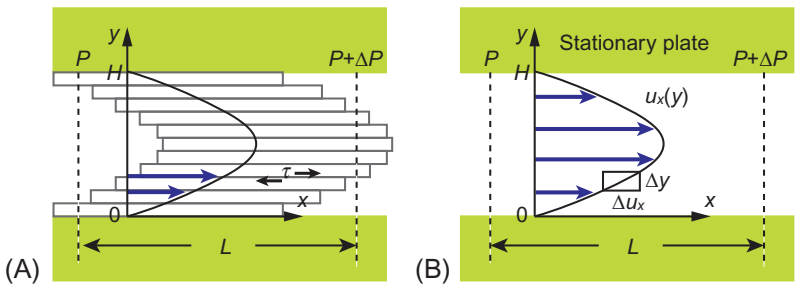

FIG. 3.6

Analysis of a laminar flow. (A) The flow can be considered to be layers of thin films. (B) Consideration of a small control volume provides the differential equation.

Unlike the case with a Couette flow, the velocity gradient is not constant. However, if we look at a layer thin enough ($\Delta y \to 0$), the same idea as the Couette flow can be used to define the viscosity (Fig. 3.6B). The local velocity gradient can be defined as:

$$\frac{\partial u_x}{\partial y} = \lim_{\Delta y \to 0} \frac{\Delta u_x}{\Delta y} \tag{3.8}$$

The shear stress acting between two adjacent layers in Fig. 3.6B is:

$$\tau(y) = \mu \frac{\partial u_x}{\partial y} \tag{3.9}$$

Eq. (3.9) can be used to form a differential equation to find the velocity profile $u_x(y)$. Eq. (3.7) is a special case of Eq. (3.9).

Laminar flow in a pipe

Let us solve the velocity profile of a stationary laminar flow in a pipe. The viscosity of the fluid is μ, the flow rate is Q, the pipe length is L, the pipe radius is R, and the pressures at $x = 0$ and $x = L$ are $P = P$ and $P = P + \Delta P$, respectively. Since the flow is laminar, we can assume that there are cylindrical layers of liquid as shown in Fig. 3.7.

Let us consider the forces acting on a thin cylindrical volume from $r = r$ to $r = r + \Delta r$ (Fig. 3.8). The force at the inside interface is:

$$F_r = -A_r \tau_r = -2\pi r L \cdot \tau_r = -2\pi r L \cdot \mu \left. \frac{du_x}{dr} \right|_r \tag{3.10}$$

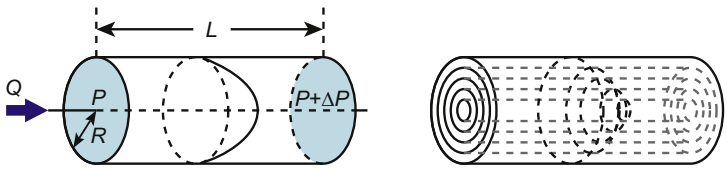

FIG. 3.7

Laminar flow in a pipe.

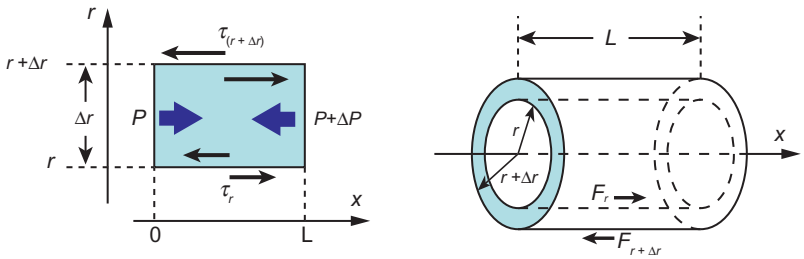

FIG. 3.8

Forces acting on a cylindrical layer.

where A_r is the area of the interface. The sign is negative because the force acts in the opposite direction of $\frac{du_x}{dr}$. In this case, the flow is faster inside, i.e., $\frac{du_x}{dr} < 0$, and the force F_r from the inside acts in the direction to drive the volume. The force at the outside interface $r = r + \Delta r$ is:

$$F_{r+\Delta r} = 2\pi(r+\Delta r)L \cdot \tau_{r+\Delta r} = 2\pi(r+\Delta r)L \cdot \mu \left.\frac{du_x}{dr}\right|_{r=r+\Delta r} \tag{3.11}$$

The force $F_{r+\Delta r}$ from the outside acts in the direction to slow down the flow. Note that the area of the interface is different from Eq. (3.10).

The actual force that drives the volume is the pressure difference between $x = x$ and $x = x + \Delta x$.

$$F_P = -\left\{\pi(r+\Delta r)^2 - \pi r^2\right\}\Delta P = -\left(2\pi r\Delta r + \Delta r^2\right)\Delta P \tag{3.12}$$

The sign is negative because when the fluid flows in the positive direction of x-axis, the pressure at $x = L$ is lower than at $x = 0$, i.e., $\Delta P < 0$. The term Δr^2 will be neglected.

Since there is no acceleration in the stationary flow, the net force is zero.

$$0 = F_P + F_r + F_{r+\Delta r} \tag{3.13}$$

Plugging Eqs. (3.10), (3.11), (3.12) into Eq. (3.13) gives:

$$-\left(2\pi r\Delta r + \Delta r^2\right)\Delta P - 2\pi rL \cdot \mu \left.\frac{du_x}{dr}\right|_r + 2\pi(r+\Delta r)L \cdot \mu \left.\frac{du_x}{dr}\right|_{r+\Delta r} = 0$$

or

$$-(r+\Delta r)\frac{\Delta P}{\mu L} + r\left(\left.\frac{du_x}{dr}\right|_{r+\Delta r} - \left.\frac{du_x}{dr}\right|_r\right)/\Delta r + \left.\frac{du_x}{dr}\right|_{r+\Delta r} = 0 \tag{3.14}$$

When $\Delta r \to 0$, this becomes:

$$r\frac{\Delta P}{\mu L} = r\frac{d^2u_x}{dr^2} + \frac{du_x}{dr},$$

which can be rearranged to:

$$r\frac{\Delta P}{\mu L} = \frac{d}{dr}r\frac{du_x}{dr} \tag{3.15}$$

Integrating Eq. (3.15) twice gives:

$$\frac{d}{dr}u_x(r) = \frac{1}{2\mu}r\frac{\Delta P}{L} + A\frac{1}{r} \tag{3.16}$$

and

$$u_x(r) = \frac{1}{4\mu}r^2\frac{\Delta P}{L} + A\,\ln(r) + B \tag{3.17}$$

Two important assumptions give the boundary conditions for Eq. (3.17).

(1) Axial symmetry: the velocity profile $u_x(r)$ is symmetric about the x axis, which requires:

$$\frac{d}{dr}u_x(0)=0 \tag{3.18}$$

(2) No slip condition: the velocity is zero at the wall:

$$u_x(R)=0 \tag{3.19}$$

From Eqs. (3.16)–(3.19), we obtain:

$$u_x(r)=-\frac{1}{4\mu}r^2\frac{\Delta P}{L}\left(R^2-r^2\right)\quad u_x(r)=-\frac{1}{4\mu}\cdot\frac{\Delta P}{L}\left(R^2-r^2\right) \tag{3.20}$$

The fluid is moving fastest at the center ($r=0$):

$$u_{\max}(r)=-\frac{1}{4\mu}r^2\frac{\Delta P}{L}R^2\quad u_{\max}(r)=-\frac{1}{4\mu}\cdot\frac{\Delta P}{L}R^2 \tag{3.21}$$

We can obtain the total flow rate by adding up the contribution from each cylinder.

$$Q=\int_{r=0}^{r=R}2\pi r\cdot u_x(r)\cdot dr=-\frac{\Delta P\pi R^4}{8\mu L} \tag{3.22}$$

In many practical cases, the flow velocity U refers to the average velocity, namely:

$$U=Q/\pi R^2=-\frac{\Delta PR^2}{8\mu L} \tag{3.23}$$

Note that U is different from the velocity at the center. The average velocity is actually half of the center velocity.

Hagen-Poiseuille equation

From Eqs. (3.22), (3.23), we obtain the *Hagen-Poiseuille equation*:

$$\Delta P=-\frac{8\mu L}{R^2}U \tag{3.24}$$

or

$$\Delta P=-\frac{8\mu L}{\pi R^4}Q \tag{3.25}$$

This equation describes the relationship between pressure, fluidic resistance, and flow rate, analogous to voltage, resistance, and current, respectively, in Ohm's law for electrical circuits ($V=RI$). Both electrical resistance and fluidic resistance are proportional to the length of the device. One important difference between the Hagen-Poiseuille equation and Ohm's law is that, unlike the electrical resistance, the fluidic resistance is not inversely proportional to the cross-sectional area πR^2, but to πR^4 (for Ohm's law, see Chapter 4, Section 4.3). The difference arises from the no-slip condition of the laminar flow. It should be noted that the Hagen-Poiseuille equation applies only to laminar flows in a pipe. As in many cases of microfluidic devices, a flow between two parallel plates is also practically important. The velocity

profile of the flow between two parallel plates is found to be parabolic, following the same steps as in the discussion in this section (see Problem 3.7).

HAGEN-POISEUILLE EQUATION

Consider stationary laminar flow in a pipe with viscosity μ, flow rate Q, average velocity U, pipe length L, pipe radius R, and pressure difference ΔP.

The Hagen-Poiseuille equation is given as: $\Delta P = -\frac{8\mu L}{R^2}U$ or $\Delta P = -\frac{8\mu L}{\pi R^4}Q$.

3.2.3 REYNOLDS NUMBER AND SCALING LAW

Navier-Stokes equations

The Navier-Stokes equations are the basic governing equations for the motion of fluid substances including liquid and gas. They relate the three-dimensional components (u, v, w) of the velocity vector $\mathbf{v}$, pressure p, and density ρ as functions of the position (x, y, z) and the time t. Because there are five unknown parameters (u, v, w, p, and ρ), five independent equations are necessary to describe a flow field. The general form of the Navier-Stokes equations consists of one continuity equation, three equations of motion (for x, y, z), and one energy equation.

Here we consider a simplified form of the Navier-Stokes equations for an unsteady incompressible flow of a Newtonian fluid, where ρ is constant.

The continuity equation is:

$$\frac{\partial u}{\partial x}+\frac{\partial v}{\partial y}+\frac{\partial w}{\partial z}=0 \tag{3.26}$$

Equations of motion are:

$$\rho\left(\frac{\partial u}{\partial t}+u\frac{\partial u}{\partial x}+v\frac{\partial u}{\partial y}+w\frac{\partial u}{\partial z}\right)=-\frac{\partial p}{\partial x}+\mu\left(\frac{\partial \tau_{xx}}{\partial x}+\frac{\partial \tau_{xy}}{\partial y}+\frac{\partial \tau_{xz}}{\partial z}\right)+f_x \tag{3.27}$$

$$\rho\left(\frac{\partial v}{\partial t}+u\frac{\partial v}{\partial x}+v\frac{\partial v}{\partial y}+w\frac{\partial v}{\partial z}\right)=-\frac{\partial p}{\partial y}+\mu\left(\frac{\partial \tau_{xy}}{\partial x}+\frac{\partial \tau_{yy}}{\partial y}+\frac{\partial \tau_{yz}}{\partial z}\right)+f_y \tag{3.28}$$

$$\rho\left(\frac{\partial w}{\partial t}+u\frac{\partial w}{\partial x}+v\frac{\partial w}{\partial y}+w\frac{\partial w}{\partial z}\right)=-\frac{\partial p}{\partial z}+\mu\left(\frac{\partial \tau_{xz}}{\partial x}+\frac{\partial \tau_{yz}}{\partial y}+\frac{\partial \tau_{zz}}{\partial z}\right)+f_z \tag{3.29}$$

Each term in the equations is explained as follows:

(1) Eq. (3.26) states that the total of the incompressible flows coming in and flowing out of a control volume $dxdydz$ should be zero, namely:

$$du\cdot dydz+dv\cdot dxdz+dw\cdot dxdy=0$$

(2) The left sides of Eqs. (3.27)–(3.29) represent acceleration, where $\frac{\partial(\ )}{\partial t}$ is the local acceleration, and $u\frac{\partial(\ )}{\partial x}+v\frac{\partial(\ )}{\partial y}+w\frac{\partial(\ )}{\partial z}$ is the convective acceleration. The term $\frac{\partial(\ )}{\partial t}$ is similar to one in a typical form of the equation of motion for a single particle,

namely $m\frac{d\mathbf{v}}{dt} = F$. In the case of fluid dynamics, substances around $P(x,y,z)$ at time $t = t$ moves to $P(x + dx, y + dy, z + dz)$ at time $t = t + dt$. In order to consider the acceleration of the substances, one has to take this translation into account.

$$\begin{aligned} d\mathbf{v} &= \mathbf{v}(x+dx, y+dy, z+dz; t+dt) - \mathbf{v}(x, y, z; t) \\ &= \frac{\partial \mathbf{v}}{\partial x}dx + \frac{\partial \mathbf{v}}{\partial y}dy + \frac{\partial \mathbf{v}}{\partial z}dz + \frac{\partial \mathbf{v}}{\partial t}dt \end{aligned}$$

Now, the acceleration can be expressed in the following way with the convective acceleration term:

$$\begin{aligned} \frac{d\mathbf{v}}{dt} &= \frac{\partial \mathbf{v}}{\partial t} + \frac{\partial \mathbf{v}}{\partial x}\frac{dx}{dt} + \frac{\partial \mathbf{v}}{\partial y}\frac{dy}{dt} + \frac{\partial \mathbf{v}}{\partial z}\frac{dz}{dt} \\ &= \frac{\partial \mathbf{v}}{\partial t} + \frac{\partial \mathbf{v}}{\partial x}u + \frac{\partial \mathbf{v}}{\partial y}v + \frac{\partial \mathbf{v}}{\partial z}w \end{aligned}$$

(3) $-\frac{\partial p}{\partial(\ )}$ in the right sides of Eqs. (3.27)–(3.29) represents the pressure gradient, which works in the same way as the discussion for laminar flow in a pipe.

(4) $\mu\left(\frac{\partial \tau_{x(\ )}}{\partial x} + \frac{\partial \tau_{y(\ )}}{\partial y} + \frac{\partial \tau_{z(\ )}}{\partial z}\right)$ is the viscous force (Fig. 3.9). Note that $\tau_{ij} = \tau_{ji}$.

(5) $f_{(\ )}$ is the volume force (or unit volume) acting on the fluid. Volume forces include gravitational force, electrostatic force, and magnetic force.

There are many cases where the Navier-Stokes equations can be expressed in much simpler forms. In fact, the Hagen-Poiseuille equation is the solution to a very simple case of a one-dimensional Navier-Stokes equation, where both the acceleration and the volume force are zero (see also Problem 3.7).

Reynolds number

The meaning of each term in the Navier-Stokes equations (Eqs. 3.27–3.29) is clearly visible in the following way, as explained in the previous section.

$$(\text{intertial force}) = (\text{pressure}) + (\text{viscous force}) + (\text{volume force})$$

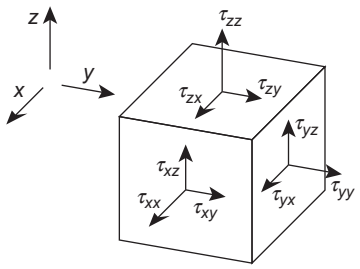

FIG. 3.9

Viscous force on a control volume.

As one can imagine, the solution to the Navier-Stokes equations are very different depending on the media (air, thin liquid, viscous liquid, etc.) and the dimensions of the flow. It is useful to find ratios between two terms to know which part plays a dominant role to define the characteristics of flow. The Reynolds number is a measure showing the ratio of the inertial force to the viscous force. It is defined by the following formula:

$$Re = \frac{Ud}{(\mu/\rho)} = \frac{Ud}{\nu} \tag{3.30}$$

where U is a characteristic velocity of the fluid and d is a characteristic length. Kinematic viscosity $\nu = \mu/\rho$, which is the dynamic viscosity divided by the density, is often used when discussing Reynolds numbers. The characteristic length, or characteristic dimension, indicates the scale of the system of concern. It has to be chosen based on the scale of the phenomenon being discussed. There are conventions for types of objects that are often considered in fluidic systems. For example, the radius or the diameter is used for spheres or circles, and the chord length is used for aircraft wings. For flow in a pipe or a microchannel, the internal diameter or an equivalent diameter is generally used. The average velocity of the object relative to the fluid is usually chosen as the characteristic velocity.

When the Reynolds number is small, the effect of the viscous force is larger, resulting in heavy damping, and the flow tends to be steadier. The Reynolds number Re is used to determine if the flow is laminar, transient, or turbulent. When the Reynolds number is small enough, the flow is laminar and we can neglect the inertial force. When the Reynolds number is large enough, the flow is turbulent and we can neglect the viscous force. In the transient region, we have to consider all the terms. For example, flow in a pipe is considered to be laminar when $R < 2300$, transient when $2300 < Re < 4000$, and turbulent when $R > 4000$. These critical Reynolds numbers change [1] depending on the criteria such as the shape of the flow, parameters to be focused, and choice of the characteristic velocity and length. As Eq. (3.30) implies, smaller systems tend to have smaller Reynolds numbers. Reynolds numbers are smaller than 10^3 for most of the microdevices or molecular sensors and the flow is considered laminar.

Reynolds numbers are also related to the behavior of creatures with different scales. Bacteria have an extremely small Reynolds number ($\sim 10^{-5}$). As the size of an animal becomes larger, the Reynolds number becomes larger (e.g., for whales, $Re = 10^{7-9}$), and the way the animal swims or flies changes (see also Problem 3.5). There are several interesting articles about the scale of animals [1a] and Reynolds numbers [2].

3.3 MICROFLUIDICS FOR MOLECULAR SENSORS

Microfluidics, as a miniaturized and high-throughput technology, has been receiving prominent attention and experiencing rapid growth. Growth in microfluidics has expanded in research towards its potential applications as well as optimization of microfluidic channel designs for specific applications. Microfluidic devices have

been utilized for lab-on-a-chip (LOC) or μTAS, where one or more laboratory functions are integrated on a single chip of centimeter to millimeter scale [3–6]. The attractive and advantageous characteristics of microfluidics include down-scaling and miniaturization. Microfluidics utilizes and consumes less fluid volumes, and requires fewer materials to make the actual device, making the device and procedures more cost-effective and capable of being mass produced [7–9]. In many situations they can be made disposable, hence creating and generating a market with constant need. Miniaturization brings molecules or samples closer together for more effective, efficient, and rapid interactions. The downsizing of microfluidic channels results in faster analysis and response times, owing to higher surface to volume ratios, shorter diffusion distances, and smaller heating capacities. Miniaturization also increases the portability of microfluidic devices because the devices are compact yet fully functional by themselves.

Microfluidics involves fluid characteristics on a small scale. When scaling down, the fundamental physics changes rapidly. Reynolds numbers are small and fluid flow is laminar, which implies no turbulence, and the geometry of the channel defines the flow field. Viscous forces tend to dominate over inertial forces, and mixing of fluid by diffusion becomes dominant over that by advection.

In this section, we introduce basics of microfluidics and practical examples of technologies that are or potentially will be utilized for molecular sensing applications.

Further reading

1. Incompressible Flow, 4th edition/Ronald L. Panton, Wiley, 2013.
2. An Introduction to Fluid Dynamics/G. K. Batchelor, Cambridge Mathematical Library, 2000.
3. Mechanics of continua/A. Cemal Eringen, Krieger Pub Co, 1980.
4. Handbuch der Physik Encyclopedia of Physics/Flügge, Siegfried.

3.3.1 MICROFLUIDIC DEVICE BASICS

Fabrication of microfluidic devices

Most microfluidic devices are fabricated by replica molding techniques [10, 11] (see Chapter 2, Section 2.5) because it allows for simple, low-cost prototyping of micro channels. Fig. 3.10 shows a typical fabrication procedure of a microfluidic chip. The polydimethylsiloxane (PDMS) microchannel is replicated from an SU-8 [12] photoresist negative pattern. Holes for tube connection are then mechanically punched through the channel. The channel is fixed onto a substrate, which often is a glass slide. There are several techniques for bonding the top micro channel and the bottom substrate. Typically, the PDMS part is O_2 plasma treated and pressed onto the glass substrate at $\sim$100°C to create permanent bonding. Simple mechanical clamps are also commonly used.

Techniques for microchannel fabrication based on lithography include bulk micromachining of silicon. Anisotropic wet etching [13, 14] or DRIE [15, 16] creates grooves on silicon substrates. Other techniques include hot embossing [17] and

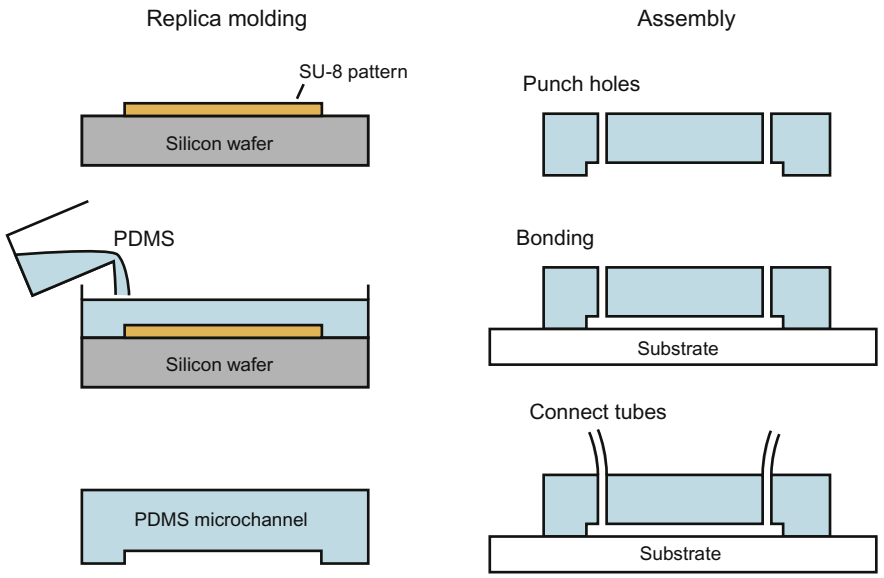

FIG. 3.10

Fabrication of a PDMS microchannel.

injection molding [18], which are suitable for mass production. See Chapter 2 for details of each method.

Pumping

Most microfluidic systems are pressure-driven by motor controlled syringe pumps or a peristaltic pump, in which rotating rollers squeeze a flexible tube. When designing a pumping device for a microfluidic channel, we need to take fluidic resistances into account. Let us take a look at the Hagan-Poiseuille law again:

$$\Delta P = -\frac{8\mu L}{\pi R^4} Q \tag{3.31}$$

It relates pressure drop and the flow rate for steady, laminar flow in a circular tube. When we scale down the radius of the pipe R to $R/2$, the pressure needed to drive the liquid at the same flow rate Q becomes 2^4 times larger. Surface-driving forces such as capillary forces or electrostatic forces are sometimes employed in accomplishing the microfluidic manipulation.

Mixing in microchannel

Diffusion and scale effect

Mixing of multiple reagents is a critical step for many of micro analytical systems. However, laminar flows in microfluidic systems make efficient mixing difficult. Laminar layers glide past each other, and the only exchange between them is

accomplished by diffusion. The *Péclet number Pe* is a dimensionless number defined as the ratio of the rate of advection by the flow to the rate of diffusion:

$$Pe = \frac{LU}{D} \tag{3.32}$$

where L is the characteristic length of the system, U is the flow velocity, and D is the diffusion coefficient. When Pe is larger, mixing by diffusion is more difficult or less efficient. Diffusion coefficient D is dependent on the diameter of particles, but is independent of the size of the mixing system. As the system becomes larger, L and U become larger and diffusion becomes less significant.

As we discussed in Section 3.2.1, diffusion length is defined as $L_D = 2\sqrt{Dt}$ ($\sqrt{2Dt}$ may be used for other boundary conditions). If we approximate $U \approx L/t$, Pe can be rewritten as:

$$Pe = \frac{LU}{D} \approx \frac{L^2}{Dt} \approx \frac{L^2}{{L_D}^2} \tag{3.33}$$

In this way, the Péclet number can be considered as a measure to compare the system lengths and the diffusion length. For example, a molecule that diffuses 1 μm in 1 ms will take 100 ms for 10 μm and 100,000 s for 10 mm. For larger systems, the Péclet number becomes larger and using diffusion for transport is unrealistic. Another good example to discuss the scale effect is the cardiovascular system of animals. Larger animals (mammals, birds, reptiles, amphibians, fish) need a circulatory system driven by a heart to transport oxygen and other substances, while smaller animals (many invertebrates such as insects) have an open circulatory system that relies on diffusion. There is an interesting argument that the distance effects on diffusion limit the maximum size of many invertebrates and skin-breathing vertebrates. Some researchers believe that the evolution of extinct giant insects was a result of the higher oxygen partial pressure, which occurred during the Carboniferous and early Permian periods [19].

Microfluidic mixers

The design of microfluidic mixers has been an important topic of microscale engineering. Even in microscale, simple diffusion may not provide sufficient mixing of liquids. Different methods have been introduced for efficient mixing in microscale [20]. One design solution to sufficient mixing is to create a serpentine channel that will mix the two fluids as they pass through the bends, as shown in Fig. 3.11.

The goal of designing an efficient micromixer is to increase the area interfacing two flows. One extension of the serpentine channel is to create a three-dimensional structure, as shown in Fig. 3.12A [21]. Fig. 3.12B shows a comparison of mixing rates with a straight channel, two-dimensional square-wave channel, and a three-dimensional serpentine channel. It shows the average intensity of reacted phenolphthalein in the three channels after the streams have been in contact for 18 mm. The three-dimensional channel produces 16 times more reaction than a straight channel and 1.6 times more than the two-dimensional square-wave channel. One

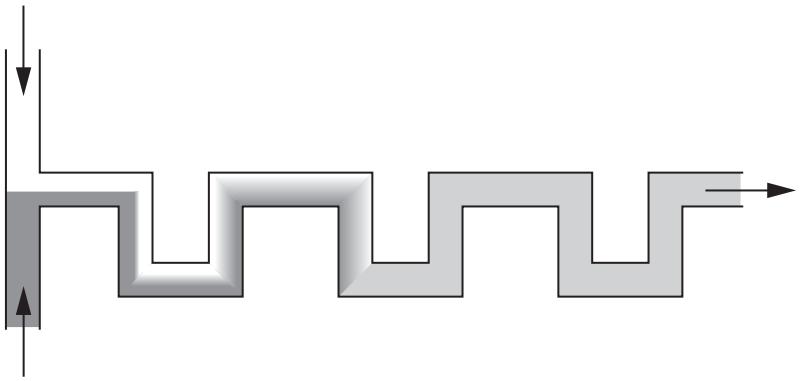

FIG. 3.11

Mixing in a serpentine microchannel.

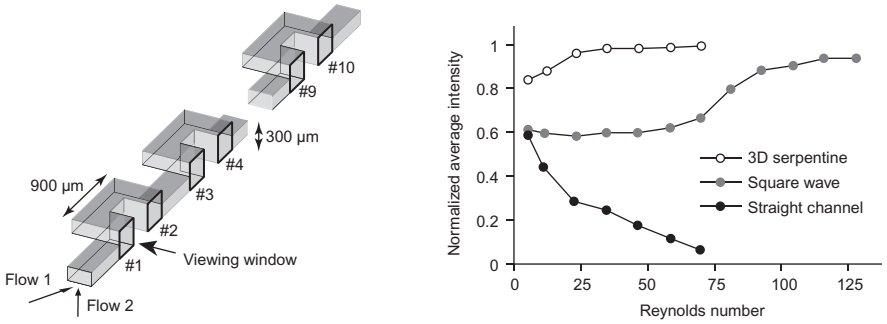

FIG. 3.12

Three-dimensional serpentine micromixer.

Adapted from R.H. Liu, M.A. Stremler, K.V. Sharp, M.G. Olsen, J.G. Santiago, R.J. Adrian, et al., Passive mixing in a three-dimensional serpentine microchannel, J. Microelectromech. Syst. 9 (2000) 190–197.

drawback in this design is the difficulty in fabrication. As we discussed in Chapter 2, photolithography only allows the design of two-dimensional structures. Multiple layers of PDMS films patterned separately were aligned and bonded to create the three-dimensional channel.

Another method is to use staggered grooves called a herringbone mixer (Fig. 3.13). The grooves are fabricated on the top wall of the channel and drive alternating helical flows. Each cycle cuts the thickness of the layers in half and doubles the interfacial area. In principle, the channel length required for mixing increases only logarithmically with the Péclet number [22].

Other methods include placing pillar-shaped obstacles in the channel. Optimization of the layout of pillar arrays is discussed in Ref. [23]. Because micro pillars or other obstacles can be easily implemented into a microchannel by a simple single mask process, it is one of the most commonly utilized designs to promote micro fluidic reactions [24, 25].

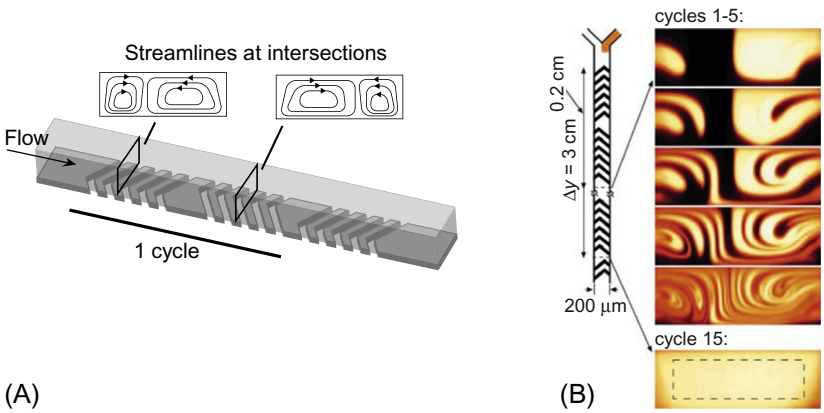

FIG. 3.13

Staggered herringbone mixer. Each cycle cuts the thickness of the layers in half and doubles the interfacial.

Part A: Adapted from A.D. Stroock, S.K.W. Dertinger, A. Ajdari, I. Mezić, H.A. Stone, G.M. Whitesides, Chaotic mixer for microchannels, Science 295 (2002) 647–651. Part B: Reprinted from A.D. Stroock, S.K.W. Dertinger, A. Ajdari, I. Mezić, H.A. Stone, G.M. Whitesides, Chaotic mixer for microchannels, Science 295 (2002) 647–651, with permission from AAAS.

The slow diffusion process can be used positively for localized transport. In a micro channel, as shown in Fig. 3.14, laminar layers glide on an intersection nearly undisturbed. By switching the flow direction, a packet of liquid of the other channel can be extracted. This packet can be used to transport a known amount of molecules or cells for analysis. An improved technique to avoid diffusion is the use of two phase flows where oil works as the carrier medium and water works as the sample medium [26].

Another interesting use of diffusion in a microchannel is the H filter. It uses different diffusivities of particles. As we discussed in Section 3.2.1, the length of diffusion can be characterized by $L_D = 2\sqrt{Dt}$, where the diffusion constant D is dependent on the size and shapes of the particles. According to the Stokes-Einstein

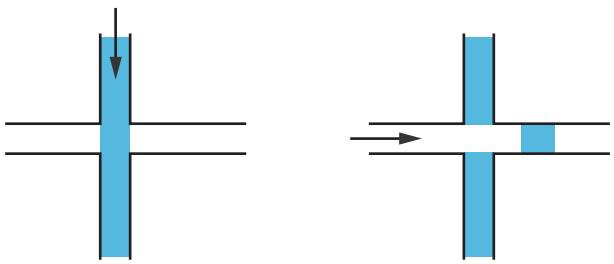

FIG. 3.14

Laminar flow allows "cropping" a part of flow.

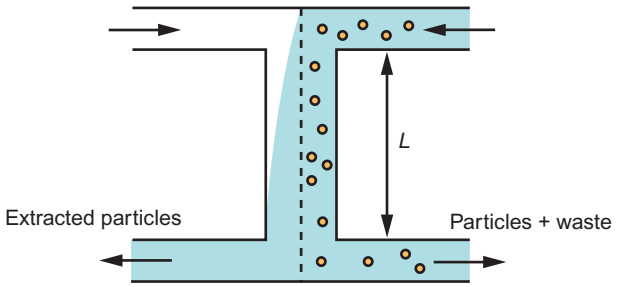

FIG. 3.15

Diagram of the H filter.
Adapted from T.M. Squires, S.R. Quake, Microfluidics: fluid physics at the nanoliter scale, Rev. Mod. Phys.77 (2005) 977.

equation, the diffusion constant of spherical particles with the radius $r$in liquid is given as:

$$D = \frac{k_B T}{6\pi\eta r} \tag{3.34}$$

where k_B is the Boltzmann constant, T is the absolute temperature, and η is viscosity.

Fig. 3.15 shows the diagram of the H filter [27]. As the medium flows through the filter, the molecules of interest, which have larger diffusivities, spread across the channel. Larger waste products have smaller diffusivities and remain confined in the initial stream [28].

IMPORTANT DIMENSIONLESS NUMBERS IN MICROFLUIDICS

Reynolds number

The ratio of the inertial force to the viscous force is:

$$Re = \frac{Ud}{(\mu/\rho)} = \frac{Ud}{\nu}$$

where U is a characteristic velocity of the fluid, d is a characteristic length, and $\nu = \mu/\rho$ is kinematic viscosity. The flow is considered to be laminar when R is small (typically when $R < \sim 10^3$).

Péclet number

The ratio of advection to diffusion, or a measure to compare the system lengths and the diffusion length, is:

$$Pe = \frac{LU}{D} \approx \frac{L^2}{Dt} \approx \frac{L^2}{{L_D}^2}$$

where L is the characteristic system length, U is the flow velocity, D is the diffusion coefficient, and L_D is the diffusion length.

3.3.2 MICROFLUIDIC CELL SEPARATION AND DETECTION

The advantages of miniaturizing bioanalytical tools include improved performance, speed, and throughput, reduced costs and reagents consumption, and the possibility of multiplexing (micro-total analysis systems). Here, we describe techniques for

microfluidic-based cell separation techniques and their applications. We first describe the principle of conventional flow cytometry or fluorescence-activated cell sorting (FACS). We shall then look at affinity-mediated cell separation, magnetic activated cell separation, electrophoresis, and mechanical property-based separation. We examine the working principles behind the various microfluidic cell separation devices and how they are implemented. We shall discuss the methods used to fabricate the various microfluidic channel-based cell separation systems, as well as the advantages and disadvantages of the techniques. Most importantly, we shall look at the different applications in which the specific technique has been used for, including important research outcomes, commercially available devices, and any novel or recent topics of interest. We also look at the various design parameters and how the improvements or changes to the parameters improve cell separation in microchannels.

Flow cytometry

Flow cytometry is a technology used to count and sort cells, and detect biomarkers [29–31]. Flow cytometry is routinely used in clinical practice, such as diagnosis of blood cancers, and is used in basic research. In a modern flow cytometer, particles (cells) pass through the observation area at a rate of several thousand particles per second and can be actively separated based on the specified optical properties.

Principles

A system for flow cytometry, or a *flow cytometer*, is a combination of (1) a flow chamber (or tube), (2) a laser-based fluorescence and/or light scattering microscope, and (3) a sorting mechanism.

(1) Hydrodynamic focusing, which locates flowing cells in the center of the chamber, is a key technique used in the flow chamber. Chamber diameters are typically hundreds of micrometers. In hydrodynamic focusing, a fluid containing cells is injected into the center of a faster-flowing sheath flow. The sheath and sample streams form a two-layer laminar flow. Because the sheath stream flows faster, the core stream velocity increases due to the viscous force acting between the two layers. On the other hand, the volume flow rate of the core stream is the same as the injection rate, reducing the cross-sectional area of the core stream. As a result, the cells are "focused" into the center of the flow chamber (Fig. 3.16A). The hydrodynamic focusing allows the cells to be in the precise focal point of the laser-based microscope.

(2) Optical microscopes are very similar to standard fluorescence and dark-field microscopes (light-scattering microscopes) in composition (see Chapter 5, Section 5.6.2 for fluorescence microscopes and Section 5.7.2 for dark field microscopes and other techniques for light-scattering microscopy). A photo multiplier tube (PMT) or an avalanche photodiode (APD), instead of a CCD in conventional microscopes, is used as the detector. Instead of recording 2D images, the PMT or APD detectors record photo intensities with higher

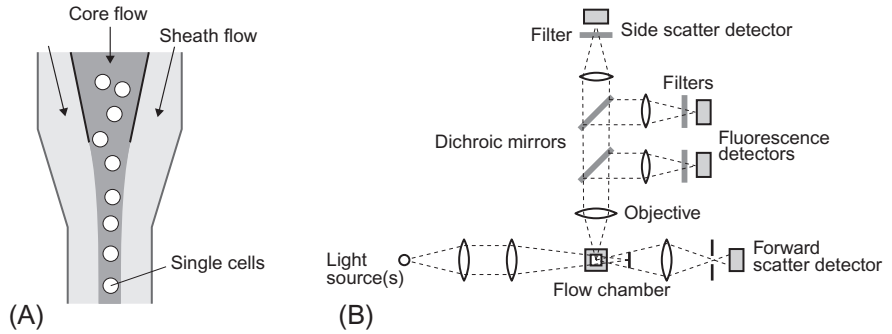

FIG. 3.16

Flow cytometer: (A) fluidic focusing and (B) optics of a flow cytometer.

sensitivity and can process thousands of cells in a second. Fig. 3.16B shows the optical observation schematic. Lasers with different wavelengths may be used for multiple fluorescent markers. A forward scatter detector (FSC) is located on the same optical axis as the laser illumination. The FSC measures forward-scattered lights, while the direct illumination is screened by a shutter. A side scatter detector may also be used, as in the figure. Side observation optics with a side fluorescence detector are used to measure fluorescence. A dichroic mirror (see Chapter 5, Section 5.6.2) reflects scattered lights and transmits fluorescence signals. It is common to integrate multiple fluorescent detectors to measure intensities of multiple markers. Multiple laser sources arranged using dichroic mirrors may be used in such cases.

(3) The sorting system is based on the technique developed for inkjet printers. Fulwyler first demonstrated successful separation of mouse and human erythrocytes in 1965. Fig. 3.17 shows the diagram of the flow cytometric cell sorting [30]: As the fluid is ejected from a nozzle as a liquid jet, the flow chamber is vibrated at typically 18 kHz to cut the fluid into a stream of droplets. Flow rates can be adjusted so that there is zero or one cell in a droplet. Each individual droplet can be either positively or negatively charged to be redirected by the electrostatic field created by two deflection plates and collected into tubes.

Commercially available systems

Flow cytometry systems from Becton, Dickinson and Company (BD) are among the most commonly used apparatuses. BD commercialized FACS, which is now a general name for flow cytometers. Other companies that produce flow cytometers include Beckman Coulter, Sony, and Millipore.

Microfluidic flow cytometry

Several attempts have been made to create fluorescence-activated microfluidic systems for cell sorting. Fig. 3.18 shows examples of microfluidic flow cytometry systems reported in the literature. In an early study by Fu et al., electro-osmotic flow was

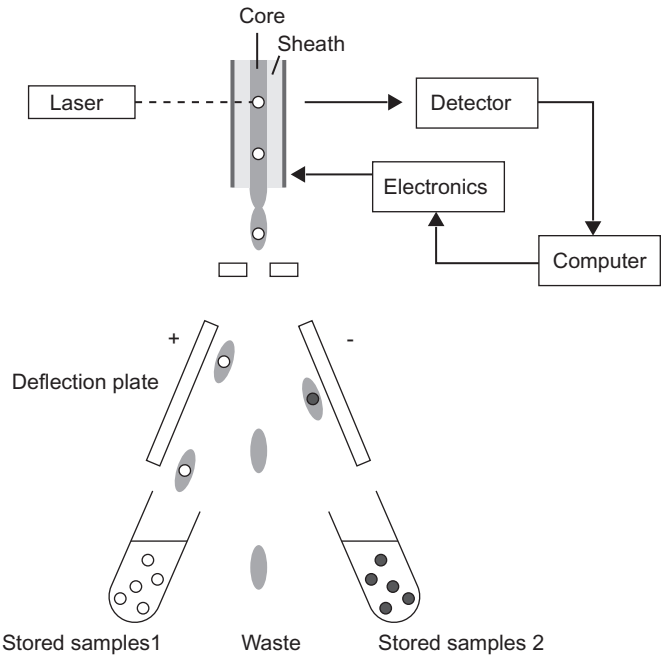

FIG. 3.17

Cell sorting mechanism.

Adapted from H.M. Davey, D.B. Kell, Flow cytometry and cell sorting of heterogeneous microbial populations: the importance of single-cell analyses, Microbiol. Rev. 60 (1996) 641–696.

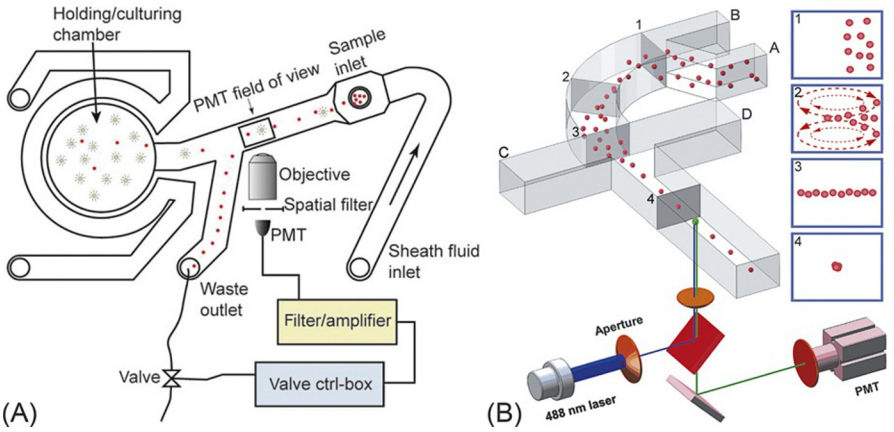

FIG. 3.18

Microfluidic flow cytometers.

Part A: Reproduced from A. Wolff, I.R. Perch-Nielsen, U. Larsen, P. Friis, G. Goranovic, C.R. Poulsen, et al., Integrating advanced functionality in a microfabricated high-throughput fluorescent-activated cell sorter, Lab Chip 3 (2003) 22–27, with permission of The Royal Society of Chemistry. Part B: Reproduced from A. Wolff, I.R. Perch-Nielsen, U. Larsen, P. Friis, G. Goranovic, C.R. Poulsen, et al., Integrating advanced functionality in a microfabricated high-throughput fluorescent-activated cell sorter, Lab Chip 3 (2003) 22–27, with permission of The Royal Society of Chemistry.

induced by applying high voltages between Pt electrodes inserted into the microchannel. The sample throughput (10–20 cells s^{-1}) was limited by the slow flow rate controlled by the applied voltages [32]. Wolff et al. used a switchable valve attached to the waste outlet and forced cells of interest to the collecting channel. The system had a high throughput (12,000 cells s^{-1}) with an acceptable 100-fold enrichment of fluorescent beads (Fig. 3.18A) [33]. Wang et al. used optical forces, which are commonly used for optical trapping of living cells, for active control of cell routing. They demonstrated sorting of HeLa cells with a throughput of ~100 cells s^{-1} with a ~60- to 70-fold enrichment [34]. It should be noted that separation, mixing, or focusing in a typical single-layer microchannel is usually designed two-dimensionally. Multilayer structures are usually needed to control flows three-dimensionally (remember the microfluidic mixing shown in Figs. 3.12 and 3.13). An interesting study made by Huang et al. developed a method of three-dimensional fluidic focusing using a two-dimensionally designed microfluidic channel [35]. Fig. 3.18B illustrates the concept. The curved section induces double-ring vortices (inset 2) in the cross-sectional plane, and sweeps the particles from the top and bottom to the center plane (inset 3). The particles in the center plane were then focused by the two-dimensional sheath flow from C and D. Another example of microchannel fabrication for flow cytometry is the use of stereolithography (see Chapter 2, Section 2.6.3) to fabricate a three-dimensional helical miniature channel for cell separation [36].

Affinity-mediated separation

Principle

Due to the natural high selectivity and specificity, antibody-antigen interactions have been widely used and integrated with microfluidic channels for cell separation purposes. Fig. 3.19 illustrates the fundamental mechanism of the affinity-mediated cell separation [37]. Antibodies are attached to the inner surface of the microchannel. When the biological samples are flown through the channel, antibodies selectively

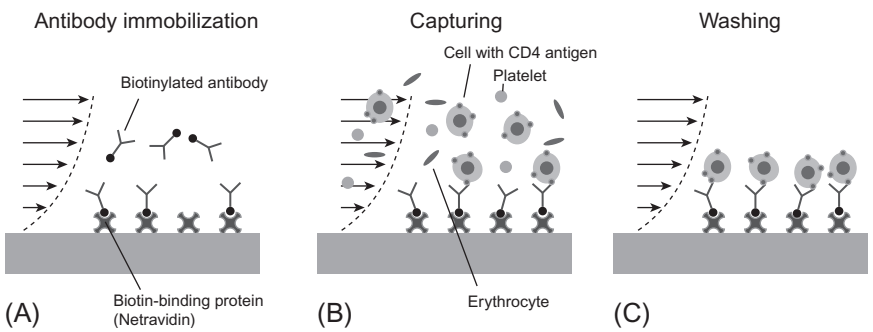

FIG. 3.19

Schematic showing an affinity-based cell separation system.

Adapted from U.A. Gurkan, T. Anand, H. Tas, D. Elkan, A. Akay, H.O. Keles, et al., Controlled viable release of selectively captured label-free cells in microchannels, Lab Chip 11 (2011) 3979–3989.

bind antigens of target cells. As a result, target cells are captured on the surface while nontarget cells flow through. The process may be followed by a washing step, where nonspecifically bound cells are removed by flowing a buffer solution.

The efficacy of the affinity-mediated separation depends on the antibody-antigen bonding between the target cells and channel substrate. Therefore, increasing the probability of physical contact between target cells and capture structure is critical in optimizing the separation performance. Meanwhile, the fluid shear stress inside the microchannel needs to be adjusted to favor target cell capture and nontarget cell removal. Methods including increasing the contact area [25, 38], and introducing in-channel mixing [39] have been demonstrated to improve the capture efficiency.

Applications

Selective cell separation from biological body fluids has broadly impacted medicine, enabling a variety of analyses with high accuracy. Several devices have been proposed for cell separation based on the cell affinity.

Moon et al. developed a portable microchip counting platform for HIV monitoring based on the $CD4^+$ T-lymphocyte counting [40]. The target $CD4^+$ cells were captured from unprocessed fingerprick volume of HIV-infected whole blood using an anti-CD4 antibody that was previously immobilized on the surface of a microfluidic channel. After capture, the cells were imaged using a lensless CCD platform with a large field of view. The shadows of cells were automatically detected and counted by an automatic recognition program. Chin et al. proposed a microfluidic system [41] that can detect HIV using only 1 μL of unprocessed whole blood. Reduction of silver ions onto gold nanoparticles in an immunosandwich procedure was adopted to amplify the signals. These types of detecting methods can be low cost, and are promising in areas where resources are limited [42].

Microchannels with different designs have been introduced to isolate rare circulating tumor cells (CTCs) from human blood samples [25, 39, 43]. Viable CTCs were separated from peripheral whole blood samples, based on the interactions between target CTCs and anti-EpCAM antibodies coated on the surface of the microchannel, without prelabeling processes. To enhance the contact between the CTCs and microchannel wall, micro-structures such as the micropillars [25], herringbone grooves [39], and 3D nanostructure [43] were designed. Another approach to improve the separation selectivity further used surface functionalization with DNA-aptamers to detect multiple types of CTCs simultaneously [44]. Aptamers that bind to a different type of cell selectively were immobilized to different regions in the microchannel. The test microfluidic device sorted different cell lines into independent fractions.

Magnetic cell separation

Principle

Magnetic separation has been utilized in microfluidic flow cytometry for increased separation. In magnetic sorting, sample cells are first incubated with magnetic particles or beads functionalized with recognition molecules, which selectively label target cells. Antibodies or nitrilotriacetic acids are typically used as the recognition

molecules. Nanoparticles or beads function as magnetic carriers to isolate cells. Cells labeled with selective magnetic carriers are separated by magnetic field gradients that trap or alter the flow of magnetic materials [45]. Magnetic sorting can be operated in either a serial or parallel manner, which results in a higher throughput. The size of the particles, or beads, tested in those studies ranged from 100 nm [46] to 4.5 μm [47] (see discussion in Chapter 2, Section 2.2). Dynabeads from Life Technologies are among the most commonly used commercially available magnetic particles.

Cell separation can be categorized into positive selection and negative selection. In positive selection, desired cells are magnetized, while negative selection labels undesired cells to be removed via magnetization. Immunomagnetic cell separation, which utilizes antibodies to target antigen molecules on the surface of the cell [48], is the most common method of magnetic cell separation. Magnetic separation is a powerful medical diagnostic tool, but is also used in laboratory settings to isolate pure sources of cells for experimental purposes. Conventionally, separation has been performed with a conical tube-based setup where strong magnets (~1 T) attract magnetized cells towards the inside wall of the tube [49]. Commercially available detection kits including MACS (magnetic-activated cell sorting) and CellSearch use the conical tube-based separation setup. MACS [49] is a general-purpose cell-sorting kit that has been utilized for various types of cells [50–54]. As of 2013, the CellSearch system [55] is the only methodology cleared by the U.S. Food and Drug Administration (FDA) for enumeration of CTCs in blood. Detection of CTCs in blood [56–60] is becoming a very important research field. We shall describe other techniques for CTC separation in later sections.

For sensor applications, cell separation with integrated fluidic devices is the main concern. Here we mainly describe magnetic cell separation performed in microfluidic systems.

Magnetic separation is affected by the level of magnetic force as well as the fluid drag force. In order for separation to occur, the magnetic force must balance the viscous drag. The magnetic force $\mathbf{F_m}$ is determined by the magnetic dipole ($\mathbf{m}$) and the magnetic field ($\mathbf{B}$) as given in the following equation [61, 62]:

$$\mathbf{F}_{\mathrm{m}} = (\mathbf{m} \cdot \nabla)\mathbf{B} \tag{3.35}$$

The total moment of a cell magnetized with magnetic carriers can be expressed as:

$$\mathbf{m} = \frac{V \Delta\chi_{\mathrm{c}}}{\mu_0}\mathbf{B} \tag{3.36}$$

where $\Delta\chi_{\mathrm{c}}$ is effective magnetic volumetric susceptibility of the cell and $\mu_0 = 4\pi \times 10^{-7}$ T m A^{-1} is the magnetic permeability of vacuum. $\Delta\chi_{\mathrm{c}}$ is found by considering a cell attached with magnetic particles as a larger single magnetic dipole, as shown in Fig. 3.20.

When N is the number of magnetic carriers attached to the cell, the effective susceptibility $\Delta\chi_{\mathrm{c}}$ is expressed as:

$$\Delta\chi_{\mathrm{c}} = N\frac{{R_{\mathrm{m}}}^3}{{R_{\mathrm{c}}}^3}\Delta\chi_{\mathrm{m}} \tag{3.37}$$

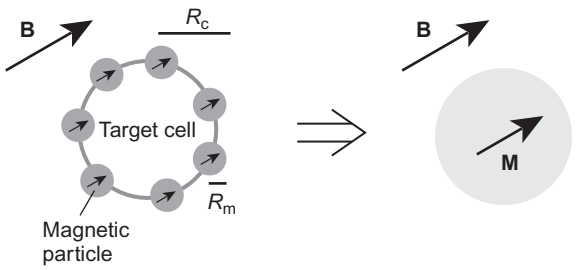

FIG. 3.20

Model of magnetic cell separation. A cell attached with magnetic particles are modeled as a single magnetic dipole.

where R_m and R_c are radii of the magnetic carrier and the cancer cell, respectively, and $\Delta\chi_m$ is the volumetric susceptibility of the magnetic carrier.

Assuming $\nabla \times \mathbf{B} = 0$:

$$(\mathbf{B}\cdot\nabla)\mathbf{B} = \frac{1}{2}\nabla(\mathbf{B}\cdot\mathbf{B}) \tag{3.38}$$

From Eqs. (3.34), (3.35), (3.37), the force acting on the cell is given in the following way [62]:

$$\mathbf{F}_m = \frac{V\Delta\chi_c}{2\mu_0}\nabla B^2 \tag{3.39}$$

where B is the magnetic field intensity, or the magnitude of the magnetic field $\mathbf{B}$.

Drag force $\mathbf{F}_d$ from the medium is given by:

$$\mathbf{F}_d = 6\pi\cdot\eta\cdot R_c\cdot\Delta\mathbf{v} \tag{3.40}$$

where η is the medium viscosity and $\Delta\mathbf{v}$ is the cell velocity relative to the medium. When we assume a quasi-static motion, the two forces equal each other, namely:

$$\mathbf{F}_d = \mathbf{F}_m \tag{3.41}$$

Substituting Eqs. (3.39), (3.40) into Eq. (3.41) and using $V = (4/3)\pi R^3$ gives the instant relative velocity of cells:

$$\Delta\mathbf{v} = \frac{R^2\Delta\chi_C}{9\mu_0\eta}\nabla B^2 \tag{3.42}$$

Eq. (3.41) defines the motion of the cell in a microchannel.

Application

Ingber et al. developed a microfluidic device which removes magnetized *Escherichia coli* bacteria from flowing solutions containing red blood cells [63]. The multiport channel shown in Fig. 3.21 is based on a typical design used for several types of microfluidics-based separation. The same group also demonstrated a blood cleansing

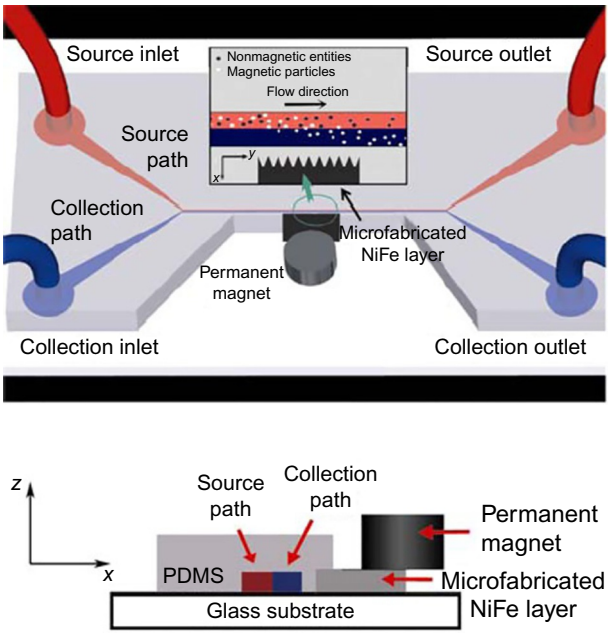

FIG. 3.21

Magnetic separation in microchannel.

Reprinted by permission from Springer: N. Xia, T.P. Hunt, B.T. Mayers, E. Alsberg, G.M. Whitesides, R.M. Westervelt, et al., Combined microfluidic-micromagnetic separation of living cells in continuous flow, Biomed. Microdevices 8 (2006) 299, Copyright 2006.

device that removes *Candida albicans* fungi from flowing human whole blood with over 80% clearance at a flow rate of 20 mL/h [64].

Furdui et al. reported an integrated silicon microchip for separation of Jurkat cells from reconstituted horse blood samples as well as human blood (about 1:10,000 ratio of Jurkat cells to blood cells) [65].

It is known that disease-infected blood cells are magnetized by themselves. They can be separated without magnetic labeling. Zborowski et al. developed a device for blood screening to test for human malaria. The device exploits the fact that *Plasmodium* species parasites produce hemozoin, which gives magnetic susceptibility to red blood cells [66].

Immunomagnetic separation of cancer cells has also been studied by several groups. Zborowski et al. demonstrated the separation of MCF7 cells (breast cancer cell line) from mixtures of human leukocytes [67]. Fig. 3.22 is the microfluidic device developed by the authors' group [68, 69].

Labeled cells are effectively captured because the microchannel is thin and flat and arrayed magnets with alternate polarities provide a sharp magnetic field gradient. Cell capture rates of 90% and 86% from whole blood flowing at 10 mL/h were demonstrated for COLO205 (colon cancer) and SKBR3 (breast cancer) cells. The

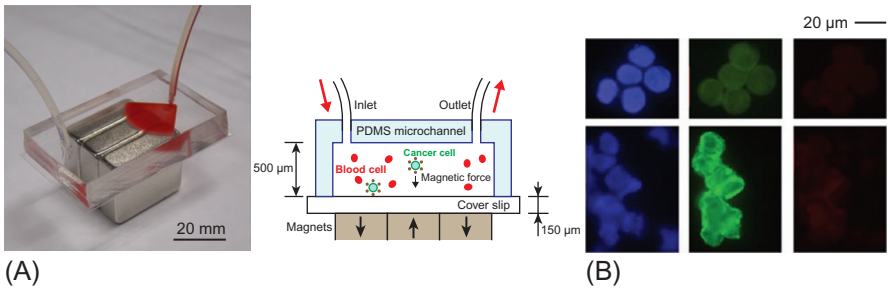

FIG. 3.22

Microchip-based immunomagnetic assay for detection of circulating tumor cells: (A) schematic of the experimental setup; (B) cancer cells captured from patient blood samples.

Part A: Reproduced from K. Hoshino, Y.Y. Huang, N. Lane, M. Huebschman, J.W. Uhr, E.P. Frenkel, et al., Microchip-based immunomagnetic detection of circulating tumor cells, Lab Chip 11 (2011) 3449–3457, with permission of The Royal Society of Chemistry. Part B: Reprinted by permission from Springer: Y. Huang, K. Hoshino, P. Chen, C. Wu, N. Lane, M. Huebschman, et al., Immunomagnetic nanoscreening of circulating tumor cells with a motion controlled microfluidic system, Biomed. Microdevices (2012) 1–9, Copyright 2012.

screening system has been tested for clinical screening and successfully isolated CTCs from the blood samples of cancer patients with breast, lung, and prostate cancers [70].

Ahn et al. developed a total analytical system that integrates components such as microvalves, flow sensors, and filters for magnetic bead-based biochemical detection [71]. Other examples of the use of magnetic force with microfluidic devices have been reviewed in the literature [72].

Electrophoresis

Principle

Electrophoresis is a technique where an applied electric field separates target cells from the medium. A particle, or a cell, suspended in a medium of different dielectric characteristics is electrically polarized in an alternating electrical field [73]. The particle polarization and the external electrical field induce a lateral dielectrophoretic (DEP) force and electrorotation (ROT). The DEP force directs the particle towards the minimum of dielectric potential, and the ROT rotates the particle. The magnitude and direction of these forces for living cells are dependent on cell characteristics such as composition, morphology, and phenotype, and can be used for cell separation. The specific capacitance of a cell membrane is given by the morphology including microvilli, membrane folds, and blebbing.

With regards to the separation mechanics, forces acting on a cell include gravitational force, DEP force, fluid drag, and hydrodynamic lift effects. The DEP force acting on a particle with a dipole moment $\mathbf{p}$ in the electric filed $\mathbf{E}$ is given as:

$$\mathbf{F}_{\mathrm{DEP}} = (\mathbf{p} \cdot \nabla)\mathbf{E} \tag{3.43}$$

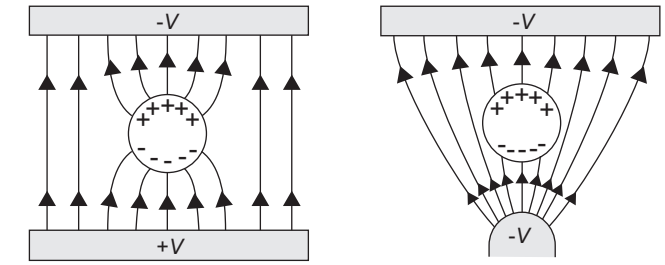

FIG. 3.23

The principle of electrophoresis.

Note that **p** is a function of **E**. Under a uniform electric field **E** between two parallel plate electrodes, the attraction forces acting on a neutral particle from the two electrodes equal each other (see Fig. 3.23A), and no net force is observed. When the two electrodes are asymmetric (see Fig. 3.23B), the two forces are different and the particle is attracted to one of them.

For the case with a cell suspended in a medium, the average DEP force can be written as:

$$\mathbf{F}_{\mathrm{DEP}} = 4\pi r^3 \varepsilon_m \alpha \cdot \nabla E^2{}_{\mathrm{RMS}}$$

or

$$\mathbf{F}_{\mathrm{DEP}} = 4\pi r^3 \varepsilon_m \alpha V^2 (k_x \mathbf{a}_x + k_x \mathbf{a}_Y) \tag{3.44}$$

where ε_m is the dielectric permittivity of the eluate, V is the peak electrode voltage, and α is the real part of the Clausius-Mossotti factor expressing the effective polarizability of the cell in the buffer. k_x and k_y are the maximum vertical and horizontal components, respectively, of the field nonuniformity factor of $\nabla E^2{}_{\mathrm{RMS}}$ for an applied 1 V peak-peak voltage. They depend on the geometry of the electrodes and the relative position of the cell. They become larger when the cell is closer to the electrodes.

The horizontal drag force from the medium is:

$$F_{\mathrm{HORIZ}} = 6\pi c r \eta (v_m - v_p) \tag{3.45}$$

where η is the dynamic viscosity, v_p is the cell velocity, v_m is the medium velocity, and $c = 1.7$ (Fig. 3.24).

The y component of $\mathbf{F}_{\mathrm{DEP}}$ and F_{HORIZ} defines the horizontal cell motion [73].

Applications

In Ref. [73], Gascoyne et al. show that breast cancer cells, MDA231, are dielectrically different from erythrocytes and leukocytes; they also demonstrate that cancerous cells can be removed from a blood sample because of dielectric differences. Each cell is dielectrically different based on its different threshold frequency. Separation chambers were constructed above electrodes. The electrode array size was 17.6 mm × 55 mm. The electrode element width and spacing were both 80 μm.

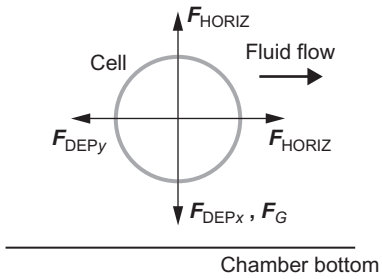

FIG. 3.24

Forces acting on a cell in a medium.

Adapted from F.F. Becker, X.B. Wang, Y. Huang, R. Pethig, J. Vykoukal, P. Gascoyne, Separation of human breast cancer cells from blood by differential dielectric affinity, Proc. Natl. Acad. Sci. 92 (1995) 860–864.

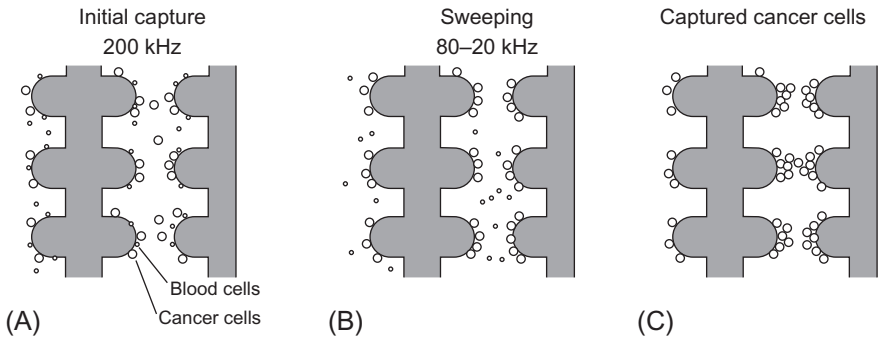

FIG. 3.25

Cancer cells captured by dielectrophoresis.

Adapted from F.F. Becker, X.B. Wang, Y. Huang, R. Pethig, J. Vykoukal, P. Gascoyne, Separation of human breast cancer cells from blood by differential dielectric affinity, Proc. Natl. Acad. Sci. 92 (1995) 860–864.

The electrode has a comb-shaped structure to create nonuniformity in the electric field to induce larger ∇E for the attraction force. An example of the electrode is shown in Fig. 3.25.

Sinusoidal voltages of fixed or swept frequencies were applied to the electrodes. Mixtures of MDA231 breast cancer cells were spiked into blood to test separation efficiency. First, buffer was filled into a chamber, and a 30 μL cell mixture was then injected. A 200-kHz signal of 5 V peak-peak voltage was applied to the electrodes to collect cells around the electrode.

After the initial collection at 200 kHz, a swept signal from 80 to 20 kHz was added to shake entrapped blood cells. A buffer solution was passed through the chamber to flush blood cells into the outlets. After 20 min, blood cells were further released by cross-flowing buffer from additional ports. Fig. 3.25 shows captured cancer cells around the electrode tips. The purity of cancer cells remaining at the electrodes was >95%.

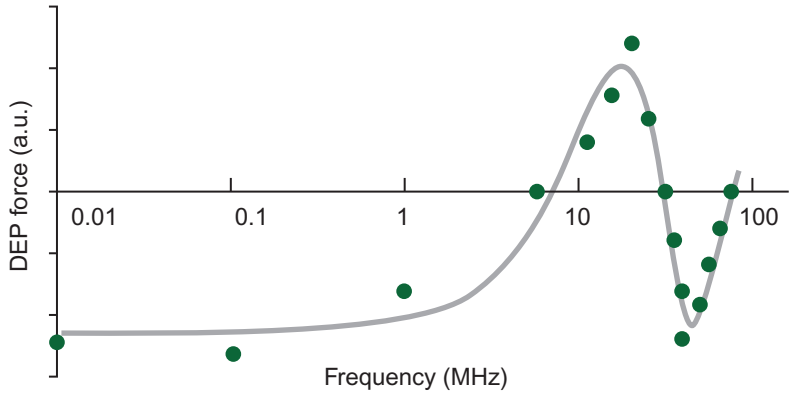

FIG. 3.26

DEP spectrum of the HCT116 cells.

Adapted from F. Yang, X. Yang, H. Jiang, P. Bulkhaults, P. Wood, W. Hrushesky, et al., Dielectrophoretic separation of colorectal cancer cells, Biomicrofluidics 4 (2010) 013204.

Yang et al. reported on the separation of colorectal cancer cells using dielectrophoresis [74]. They designed a DEP colorectal cell separation system with two electrodes at the bottom surfaces of the microchannel. The electrode pair is in parallel and has a 45° angle to the stream-wise direction in the main channel. Alternating current electric signals are applied to the two electrodes. The operation principle was that negative DEP force acts on the target cells and repels them against the main stream. There is a side channel placed near the electrode gap at one side of the main channel. The channel carries the target particles that are separated from other particles in the main channel by the negative DEP force. The important part is finding a frequency that gives a negative DEP force specifically for cancer cells. Fig. 3.26 shows the DEP forces on the HCT116 cells measured for different signal frequencies. The cancer cells experience a negative force in the frequency band of 1 Hz to 6 MHz and 31–75 MHz, and experience a positive DEP force in the frequency range of 6–31 MHz.

Cell separation utilizing mechanical properties

Acoustic separation

Acoustic separation, or acoustophoresis, is the method that separates particles using high-intensity sound waves. Standing wave based cell separators have been promoted as a means for contactless handling and manipulation of cells [75–79]. Contactless manipulation eases the physical stresses and forces experienced by cells in the microfluidic channel, thereby preserving the viability of the cells and allowing for retrieval and postanalysis.

Laminar flows in the microscale domain make the fractionation systems created by acoustic forces more efficient in continuous flow particle separation. Furthermore, microchannels require reduced resonator dimensions, resulting in higher

resonance frequencies. Higher resonance frequencies yield stronger radiation forces on particles because the primary radiation force is proportional to the frequency. Particle focusing and separation performance are both improved. However, standing wave-based microfluidic separators are limited by channel geometry and particle geometry. As the particles become smaller, the primary radiation force rapidly decreases. Therefore, only particle sizes of about tenths to tens of micrometers can be manipulated by the primary radiation force within aqueous-based solutions. Other physical parameters such as sedimentation and channel occlusion can also affect the performance of the primary radiation force [80].

Acoustic cell separation in a microfluidic channel begins with suspended particles in medium entering the rectangular cross-section channel, through an inlet. A piezo-ceramic actuator is used to generate a half-wavelength acoustic standing wave between the side walls of the microchannel, which creates an acoustic force field that is perpendicular to the flow direction (see Fig. 3.27A). The acoustic force moves the particles or cells laterally across the channel towards the center as they flow down the channel length. The rate at which they laterally translate is dependent on the particle size, density, compressibility, and acoustic pressure amplitude. Most rigid particles and cells are moved to pressure nodes. Liquid elements or bubbles move to anti nodes.

The key principle of acoustic separation is to create a particle or cell gradient across the channel at the channel end in order to sort and separate various particles and cells correctly (see Fig. 3.27B).

Various parameters that were of major consideration were channel length, the power applied to the piezoelectric element, and the axial acoustic primary radiation force (PRF). The channel length was determined by the desired flow rate, particle mixture used, and the acoustic input power. The power applied to the piezoelectric element was determined based on the size of the particles and the desired lateral displacement of the particle type. The axial acoustic PRF was the main driving force of the separation process. The magnitude of the axial PRF, F_r, is dependent on the

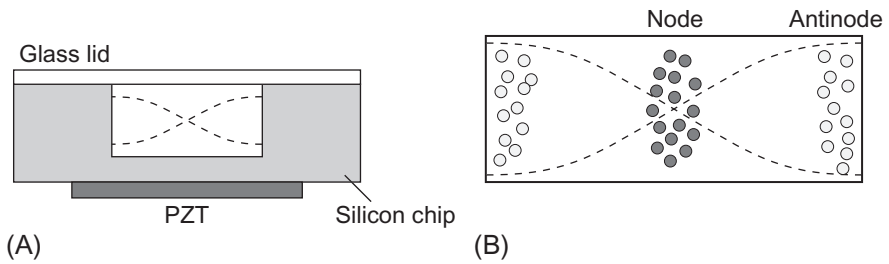

FIG. 3.27

Acoustic cell separation: (A) schematic of an acoustic separation chip and (B) particles are separated based on size and density.

Adapted from T. Laurell, F. Petersson, A. Nilsson, Chip integrated strategies for acoustic separation and manipulation of cells and particles, Chem. Soc. Rev. 36 (2007) 492–506.

properties of the medium and the particles, and the amplitude and wavelength of the standing wave. These dependencies can be described in equations given by the following:

$$F_r = -\left(\frac{\pi p_o^2 V_p \beta_m}{2\lambda}\right)\phi(\beta,\rho)\sin(2kx) \tag{3.46}$$

$$\phi = \frac{5\rho_p - 2\rho_m}{2\rho_p + \rho_m} - \frac{\beta_p}{\beta_m} \tag{3.47}$$

where φ is the particle's acoustic contrast factor, ρ_m is the density of the medium, ρ_p is the density of the particles, β_m is the compressibility of the medium, β_p is the compressibility of the particles, p_o is the pressure amplitude, V_p is the volume of the particle, λ is the ultrasonic wavelength, k is $2\pi/\lambda$, and x is the distance from a pressure node. The magnitude of the axial PRF is the primary factor in determining the rate of particle movement perpendicular to the flow direction.

The first term of the right-hand side of Eq. (3.46) states that the force is proportional to the volume of the particle and the squared acoustic amplitude, which is related to the power supplied to the piezoelectric ceramic. Along with axial PRF, the opposing viscous drag force (see Eqs. 3.40, 3.45) also plays a role in determining the rate of particle movement [14, 75, 81, 82].

Fig. 3.28 shows a top-view illustration of microchip-based acoustic separation reported by Laurell et al. Particles with negative φ factors are collected in the central part of the flow, while particles with positive φ factors are moved to the sides of the channel to be separated. Separation efficiencies of >95% were demonstrated with a flow rate of 0.3 mL min^{-1}, an actuation voltage of 10 Vpp, and an actuation frequency of ~2 MHz. One application that Laurell et al. studied is removal of human lipid (fat) particles from a suspension of red blood cells, simulating blood washing needed in open-heart surgery. They used a sonicated emulsion of tritium-labeled trioleine in saline solution as test lipid particles. With the optimized operation condition described above, they demonstrated that 85% of the lipid particles added to 1% by volume were removed independently of the concentration of erythrocytes which

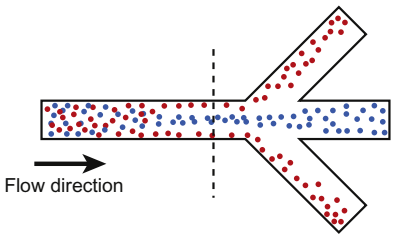

FIG. 3.28

Separation of particles with negative (blue) and positive (red) φ factors.

Adapted from T. Laurell, F. Petersson, A. Nilsson, Chip integrated strategies for acoustic separation and manipulation of cells and particles, Chem. Soc. Rev. 36 (2007) 492–506.

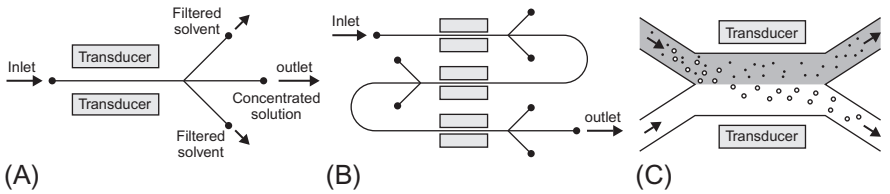

FIG. 3.29

Schematic of the acoustic cell separators by Kapishnikov et al.: (A) one-stage microchannel; (B) three-stage microchannel; (C) cell size sorter.

Adapted from S. Kapishnikov, V. Kantsler, V. Steinberg, Continuous particle size separation and size sorting using ultrasound in a microchannel, J. Stat. Mech. Theory Exp. 2006 (2006) P01012.

ranged from 2.5% to 10.0% by volume. They used the concept of increasing the throughput by using several parallel channels.

The microchip designed by Kapishnikov et al. [83] was used to perform particle size sorting in a size spectroscope, rather than just a separator. The device operates on the same working principle as the previous device [80]. The use of the standing wave field can cause particles to accumulate in the nodes of the acoustic force and is dependent on particle properties and acoustic frequency and wavenumber. The microchannels were produced via soft lithography techniques using SU-8, a UV-sensitive epoxy. The microfluidic chip itself was made of silicone elastomer. Two designs were investigated. In the first design, separation of particles occurs between two parallel transducers located in the inlet and produces the standing wave (see Fig. 3.29). The filtered pure solvent is removed via two side outlets while the concentrated solution with particles is removed via the central middle channel. The second design is a three-stage device that works in a similar way with particle separation occurring on each stage of the separator. Particles affected by the standing waves are removed via the two side outlets while the concentrated solution flows into the central channel and into the next stage for more dilution and separation. At each stage, the flow rate is three times less than the previous stage, which improves the filtering efficiency. The cell size sorting component is another microchannel and operates on the idea that particle velocity depends strongly on the size; therefore, larger particles will move faster through an interface between a pure solvent and solution of different size particles [83].

Despite the successful separation of particles and cells within the laboratory settings, microfluidic acoustic cell separation has seen little advancement in clinical settings. Compared to more developed techniques such as fluorescence-activated cell separation, microfluidic acoustic cell separation is less reliable [84]. Because the method is extremely reliant on physical parameters, such as the particle or cell size and density, that are hard to control, the piezo-ceramic actuation must be precise and actuate at the correct fundamental frequency in order to separate the particles and cells effectively. The piezo-ceramic actuation must actuate at the right frequency to generate the gradient across the microfluidic channel upon which the separation

is based. In large part, quantifying particle separations performed by acoustic separation remains challenging and validating methodology performance is equally difficult. Especially when working with particles of micron sizes, the ability to distinguish effectively between different particle sizes dramatically decreases and the noise level rises [84].

Separation based on stiffness

In the next two sections, we discuss cell separation methods that utilize direct mechanical interaction between cells and the device. This section discusses separation based on the stiffness of the cell. In Ref. [85], Zhang et al. developed a microfluidic chip to separate and enrich cells based on their deformability. The cells were also analyzed using fluorescence microscopy, flow cytometry, and assays to determine the qualities of their phenotype [85]. The separation chip, which was fabricated based on PDMS soft lithography, utilizes artificial microbarriers and hydrodynamic force to separate deformable cells from stiff cells (Fig. 3.30).

The separation occurred due to differences in deformability, while the cells also differ in their metastatic potential. Their work was applied to separate breast cancer cells MDA-MB-436 and MCF-7, which have distinct deformabilities and metastatic potential. More importantly, Zhang et al. separated a heterogeneous cancer cell line SUM149 into flexible and stiff subpopulations and analyzed their gene expression. The flexible population is associated with overexpression of genes that contribute to cancer formation. Their results suggested that tumor-initiating cells are more deformable and they are less differentiated in terms of cell biomechanics [85].

Another group has employed microfluidics to perform passive sorting and separation of cells by deformability [86]. Their technology employs microfluidic filters in series with pore sizes decreasing incrementally. As the cells flow through the device, the cells experience stresses that are similar to when they pass through capillary beds [86].

Separation based on size

Three main techniques are used to sort cells based on size: hydrodynamic sorting, microfilters, and centrifugation.

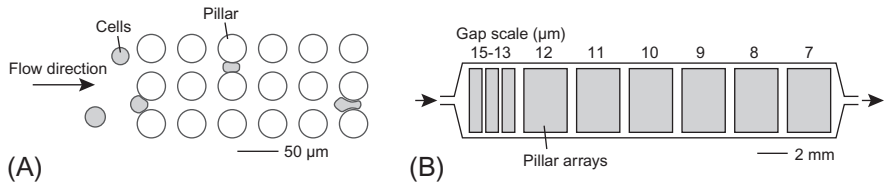

FIG. 3.30

Cancer cell sorting based on deformability.

Adapted from W. Zhang, K. Kai, D.S. Choi, T. Iwamoto, Y.H. Nguyen, H. Wong, et al., Microfluidics separation reveals the stem-cell-like deformability of tumor-initiating cells, Proc. Natl. Acad. Sci. 109 (2012) 18707–18712.

Davis et al. separated white blood cells, red blood cells, and platelets from blood plasma at flow velocities of 1000 μm/s and volume rates up to 1 μL/min [87]. They utilized a size-based hydrodynamic separation method previously introduced by the group in Ref. [88]. The method is based on a flow channel, which they call a continuous-flow deterministic array. A particle smaller than a critical hydrodynamic diameter D_c follows streamlines cyclically through the gaps, moving in an average downward flow direction, staying within a flow stream. A particle larger than the critical diameter does not fit into the first streamline and is moved by hydrodynamic lateral drag and displaced into the next streamline at each obstacle. Streamlines for both a small particle and a large particle are shown in Fig. 3.31.

Microfilters can separate cells based on a combination of size and cell deformability. Some microfilters use micropores, which act as sieves [89–91]. Fig. 3.32 is an example of cancer cells separation from blood reported in Ref. [90].

CTCs are typically in the size range of 12–25 μm. Leukocytes, which compose most of the blood cell population, are typically in the size range of 7–15 μm. Size-based sorting is attractive because there is no sample preparation necessary and no labels are needed. The largest problem is the specificity. Size-based selection leaves types of cells that are morphologically similar to CTCs, and fails to find cancer cells that are as small as leukocytes. Clogging of blood cells is a practical problem associated with this method.

Centrifugation uses centrifugal force as the force of separation and can separate cells based on their density. For an example of blood cell separation, leukocytes (white cells), thrombocytes (platelets), and cancer cells are sorted in a thin layer called the buffy coat between the layers of erythrocytes (red cells) and plasma. There are types of density centrifugation media including Ficoll and OncoQuick [92].

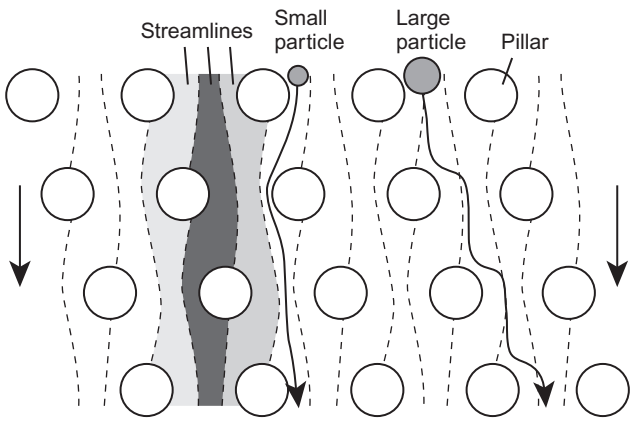

FIG. 3.31

Hydrodynamic separation based on size.

Adapted from J.A. Davis, D.W. Inglis, K.J. Morton, D.A. Lawrence, L.R. Huang, S.Y. Chou, et al., Deterministic hydrodynamics: taking blood apart, Proc. Natl. Acad. Sci. 103 (2006) 14779–14784.

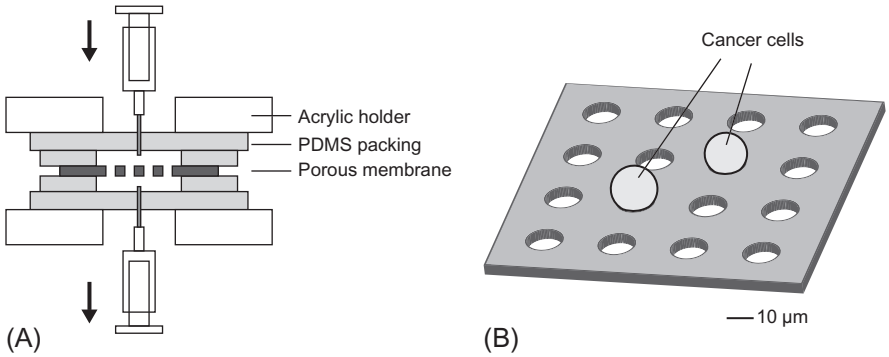

FIG. 3.32

Size-based separation.

Adapted from H.K. Lin, S. Zheng, A.J. Williams, M. Balic, S. Groshen, H.I. Scher, et al., Portable filter-based microdevice for detection and characterization of circulating tumor cells, Clin. Cancer Res. 16 (2010) 5011–5018.

METHODS FOR MICROFLUIDIC CELL SEPARATION

Immunoassay-based methods
- Flow cytometry, fluorescence-activated cell sorting (FACS)
- Magnetic separation, magnetic-activated cell sorting (MACS)
- Affinity-mediated separation

Utilization of electrical properties
- Electrophoresis

Utilization of mechanical properties
- Acoustic separation
- Size-based separation (hydrodynamics microfilters, centrifugation)

Stiffness-based separation

3.3.3 MICROFLUIDIC DEVICES FOR DNA ANALYSIS

DNA analysis is important for detecting diseases and mutations. It is now possible to determine whether a patient carries a genetic disorder or has a certain gene, or even to perform a paternity test using DNA analysis. There are several fundamental techniques used for DNA analysis including detection, amplification (polymerase chain reaction or PCR), and separation (electrophoresis). Furthermore, there is a continuous search for more efficient ways to perform these and other key steps in DNA analysis. Many steps can now be carried out in microfluidic devices. Microfluidics has the potential to make DNA analysis faster, more efficient, less expensive, and more accurate.

For DNA detection, gene microarrays and other microsystems are becoming more widely available. Microarrays allow for very large numbers of reactions to occur simultaneously within a very minute area, eliminating the need for large amounts of materials, equipment, and manpower. There have also been many

advances in miniaturizing PCR as well as different electrophoretic methods. The aim of microfluidic devices in DNA analysis is to create a complete system in which DNA can be analyzed on a single chip. Ideally, one device would be able to perform separation of samples and PCR, and detection of DNA.

Microfluidic devices for DNA amplification

DNA amplification is an essential first step for DNA analysis. The PCR is generally the method used to perform DNA amplification, but the conventional method of PCR is often time-consuming, expensive, and carries high risks for contamination [93]. With the advent of microfabrication technology, the development of microscale PCR devices has been possible. Micro-PCR offers advantages including less use of reagents, rapid cooling/heating rates, decreased power consumption, and portability. The idea of the LOC system is increasingly popular, and incorporating PCR in these devices will greatly improve efficiency and will greatly develop microfluidic diagnostic devices. PCR microfluidic devices allow for multiple reactions to occur simultaneously while decreasing the risk of contamination and increasing efficiency [94].

Principles

The PCR, invented by Kary Mullis in 1983, is a tool used to amplify a DNA sequence exponentially. To amplify the target DNA segment, two primers, a forward and reverse primer, are designed to complementary base pair with the leading and lagging parts of the target DNA. Primers, which are generally 18–30 bases long, are mixed into an aqueous solution containing the target DNA, reaction buffer, heat-stable DNA polymerase, deoxynucleoside triphosphates (dNTPs), and magnesium. PCR amplification is separated into three steps: denaturation, annealing, and extension, as illustrated in Fig. 3.33.

(1) The target DNA sequence is denatured to two single strands by heating the sample to about 98°C for 30–120 s.
(2) The temperature is typically decreased to between 55°C and 65°C for 20 s, to allow the primers to anneal to the target DNA. The annealing temperature is about 5°C below the melting temperatures of the primers.
(3) The temperature is increased to 70–80°C for about 25 s per kilobase of target DNA length and the DNA polymerase extends the primers by adding the appropriate dNTP.

The three-step amplification process is then repeated for 20–30 cycles to obtain a high quantity of target DNA. Issues associated with PCR include amplification of nonspecific PCR products if the primers hybridize to noncomplementary sequences. One potential by-product of PCR is primer dimers, primer molecules that hybridize to each other instead of matching with the target DNA.

There have been several approaches to realize microfluidics-based PCR systems. As described above, the key technologies required for microfluidic PCR is a

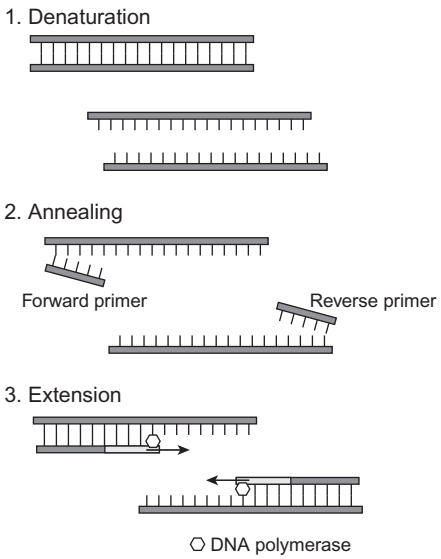

FIG. 3.33

Polymerase chain reaction (PCR).

capability of repeated precise temperature control and handling of a small amount of liquid volumes without contamination.

During PCR, the reaction mixture undergoes many cycles of varying temperature. Thermal cycling in a microfluidic device is implemented in two main ways. Fig. 3.34 illustrates the two types of PCR microfluidic devices. The one to the left represents the stationary chamber type [95] and the one to the right represents the flow-through type [96]. In the stationary PCR device, there is a PCR inlet and outlet, where the solution flows through the device, and there are chambers in which the temperature can be controlled. An early stationary microfluidic PCR device was reported by Northrup et al. [97, 98]. This device contains heating elements with coils, which are heated by an electrical current. This type of device is generally made of silicon, glass, PDMS, PMMA, polycarbonate, polyimide, or epoxy. In the flow-through PCR device, the reaction mixture is pumped through the channel. The temperature goes through three temperature zones necessary for PCR amplification multiple times. The idea of flow-through PCR was first introduced by Nakano et al. [99]. On-chip serpentine rectangular channel-based flow-through PCR microfluidics is currently the most popular implementation. The device was first conceived by Kopp et al. in 1998 [95].

There are various methods for fabrication of PCR microfluidics devices. Those generally used have been silicon/glass-based or polymer-based microfabrication methods. Silicon is the better choice for PCR devices because its higher thermal conductivity allows rapid thermal cycling. Silicon/glass-based devices are generally made by basic silicon micromachining techniques, which include photolithography,

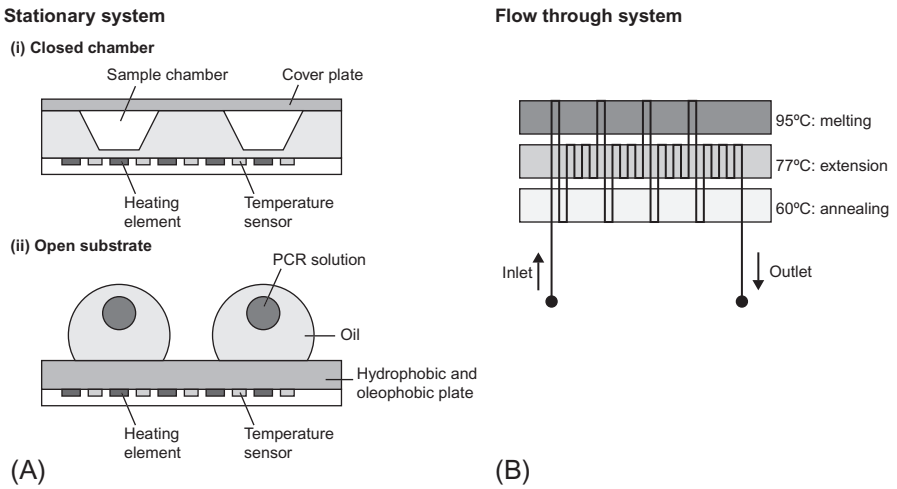

FIG. 3.34

Microchip-based PCR devices.

Part A: Adapted from M.U. Kopp, A.J. de Mello, A. Manz, Chemical amplification: continuous-flow PCR on a chip, Science 280 (May 15 1998) 1046–1048. Part B: Adapted from C. Zhang, D. Xing, Miniaturized PCR chips for nucleic acid amplification and analysis: latest advances and future trends, Nucleic Acids Res. 35 (2007), 4223–4237.

thermal growth of silicon oxide, chemical etching, electrochemical etching, ion etching, chemical vapor deposition, physical vapor deposition, epitaxy, and anodic bonding [100]. A significant drawback is the higher cost of fabrication and optical opacity, which makes microscopic analysis difficult. The use of polymers such as PDMS or PMMA has emerged as a cheaper, more biocompatible alternative than silicon, and is the current candidate for building disposable microfluidic PCR devices. Drawbacks of PDMS include the loss of sample due to its high permeability as well as bubble formation due to its inherent hydrophobicity. Microfluidic channels can be made using soft lithographic techniques.

Applications

Conventional PCR techniques have been used to quantify viruses and bacteria. Applications include analysis of HIV-1 RNA levels in plasma [101], hepatitis B and C viruses [102], human papillomavirus [103], chlamydia trachomatis infections from urine samples [104], Neisseria gonorrhoeae [105], and cytomegalovirus [106]. PCR microfluidic devices have the potential to expand the use of PCR into wider fields of research and clinical applications. One significant goal is efficient and accurate DNA detection. As PCR microfluidic devices are able to handle small volume of samples accurately, they can be more effective at detecting DNA and are less prone to contamination. These devices will amplify the DNA of the sample and detect target DNA for diagnosis of diseases such as human immunodeficiency virus,

human papillomavirus, hepatitis virus, Salmonella typhimurium, M. tuberculosis, and malaria [107]. The devices can also be used to detect and identify hereditary genetic disease, *E. coli*. Microbial detection, and other various biological agents. Because the basic principle is the amplification and detection of specific DNA, there are many applications [108]. A microfluidic digital PCR device was created to enable multigene analysis of environmental bacteria [109]. The device allows for rapid separation and partitioning of single cells from a complex sample, and represents a major breakthrough in environmental science, because microbial species can be easily identified.

Implementation and commercial products

Several approaches have been reported on integrating PCR devices into μTAS [110–113]. An early, and excellent example of a fully integrated PCR system is reported by Liu et al. [110]. This μTAS can automatically perform every step of analysis, including sample preparation, cell preconcentration and purification, PCR, and electrochemical detection. It has been proven to detect pathogenic bacteria in human blood samples and single nucleotide polymorphisms as well. The device contains a plastic fluidic chip, a printed circuit board, and a sensor microarray chip, as shown in Fig. 3.35. The chip is 60 × 100 × 2 mm in size and contains channels and chambers that are 0.5–1.2 mm deep and 1–5 mm wide. The chip is made out of polycarbonate using computer-controlled machining. Electrochemical pumping was achieved by adding 0.5-mm diameter platinum wires and placing them in contact with wells

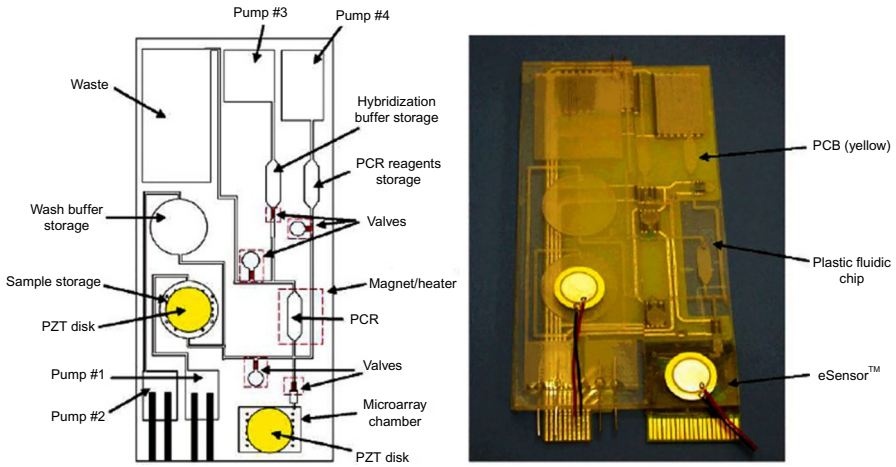

FIG. 3.35

Integrated biochip with PCR functionality.

Reprinted with permission from R.H. Liu, J.N. Yang, R. Lenigk, J. Bonanno, P. Grodzinski, Self-contained, fully integrated biochip for sample preparation, polymerase chain reaction amplification, and DNA microarray detection, Anal. Chem. 76 (2004) 1824–1831, Copyright (2004), American Chemical Society.

containing NaCl solutions. Thermally actuated micro-valves [114] were made by melting paraffin into the channels.

First, the sample is incubated with immunomagnetic capture beads so target cells can be labeled. The sample is then flowed into the PCR chamber, where the labeled cells will be trapped by a magnet, while the unlabeled solutes are washed away. The device is able to achieve complete mixing of a 50 μL chamber in 6 s and the target cell capture rate was 73%. The separated cells then undergo thermal lysis to extract the DNA and PCR is performed. After PCR, a hybridization buffer is added to hybridize the target DNA amplicon. A redox reaction occurs during hybridization, which is detected by the platinum wires and measured voltametrically. The device is able to detect *E. coli* from rabbit blood in 3.5 h. It was able to detect a single polymorphism in 2.7 h.

The Fluidigm BioMark System was introduced in 2006 as the first commercial system for digital PCR based on integrated microfluidic microchips with integrated chambers and valves for partitioning samples. The underlying microfabrication technique was developed in 1998 by Quake et al. at the California Institute of Technology, called Multilayer Soft Lithography (MSL). In this process, the soft silicone elastomer used to produce the microfluidic device deflects under pressure, creating an effective seal or valve that cuts off fluid flow within the channel (see Fig. 3.36) [115]. The valve forms the foundation behind the Fluidigm's many integrated microfluidic circuits, trademarked as the NanoFlex valve. The development of NanoFlex valves aided in the advancement in fluid manipulation as a precise, low-cost microscale platform capable of gentle and efficient handling of samples and reagents.

The Fluidigm BioMark System is one of the many microfluidic systems produced by Fluidigm that utilizes the NanoFlex valve on an integrated microfluidic microchip for single-cell gene expression profiling using digital PCR, genotyping, mutant detection, and real-time PCR. The automated system is capable of performing the essential steps of genotyping and PCR workflow including thermal cycling and fluorescence detection. It is ultimately a multiplexor, a combinatorial array of binary valve patterns, which controls the flow of fluids on the microchip. The number of

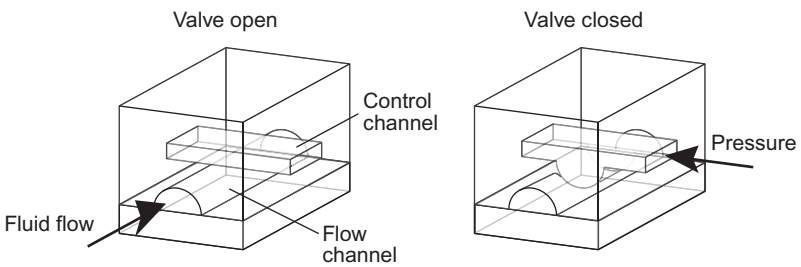

FIG. 3.36

NanoFlex valves microfabricated using a multilayer soft lithography technique.
Adapted from S. Haeberle, R. Zengerle, Microfluidic platforms for lab-on-a-chip applications, Lab Chip 7 (2007) 1094–1110.

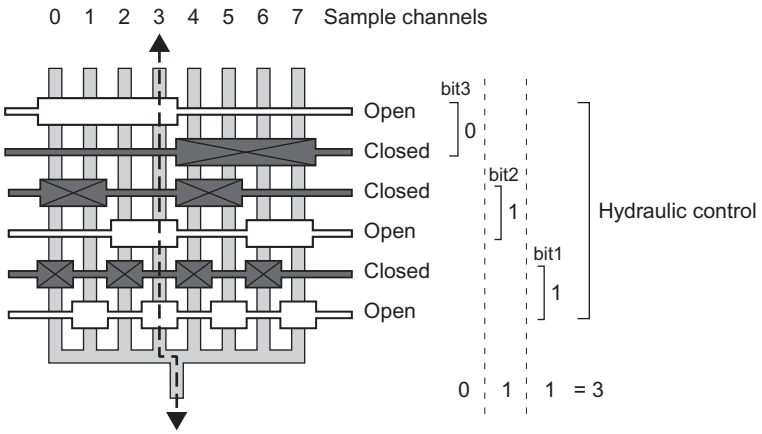

FIG. 3.37

Optical micrograph of a microfluidic chip loaded with colored food dye.

Adapted from T. Thorsen, S.J. Maerkl, S.R. Quake, Microfluidic large-scale integration, Science 298 (2002) 580–584.

control channels is logarithmically proportional to the number of flow channels, enabling high throughput through fewer controls. A device can contain thousands of channels and valves, but controlled through small numbers of inlets. Fig. 3.37 shows the concept of microfluidic multiplexing based on NanoFlex valves. It uses the idea of binary coding. In this example, each pair of hydraulic control represents a "bit" and makes a half of the eight sample channels closed by pressurization and the others open. The combination of the three bits allows the multiplexing of 2^3 lines [116]. This multiplexing and high-throughput capability enable handling of samples and primer-probes sets for up to $96 \times 96 = 9216$ PCR reactions. Fig. 3.38 shows a photograph of a chip for 48×48 reactions [117]. A typical digital PCR run using the BioMark system involves manual preparation, priming and pipetting samples into inlets on the chip, after which all mixing, thermal cycling, and fluorescence detection are performed automatically on the chip. As of 2013, the system does not have FDA or other similar regulatory body approval, and the use is limited for research use only.

The chip is first primed using the NanoFlex integrated fluidic circuit (IFC) controller, which pressurizes the control lines and closes the interface valves (IV) to prevent sample mixing. Samples and gene expression assays are individually pipetted into sample inlets and detector inlets, respectively. The chip is then loaded onto the NanoFlex IFC controller for loading and mixing, during which a pressure is applied to the fluid in the sample inlets and the fluid is pushed into fluid lines and individual wells. Simultaneously, the detector inlets are pushed into the fluid lines, prevented by IVs from mixing. Containment valves (CV) are then closed and IVs are opened, pushing reagents in the detector inlets into individual reaction chambers for mixing. After mixing, the IVs are closed and thermally cycled, a process that takes about 55 min [4].

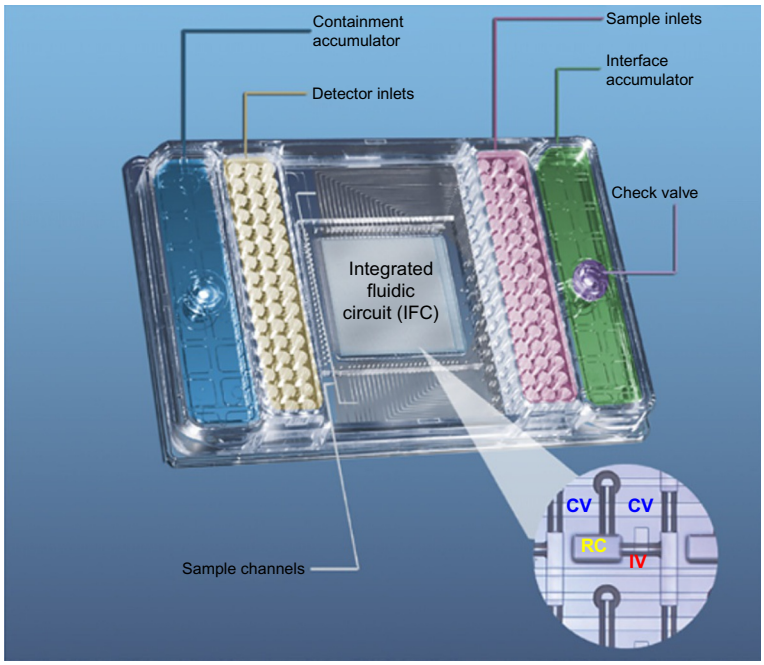

FIG. 3.38

The array chip.

Reprinted from S.L. Spurgeon, R.C. Jones, R. Ramakrishnan, High throughput gene expression measurement with real time PCR in a microfluidic dynamic array, PLoS One 3 (2008) e1662.

The BioMark System has been used by many as an integrative part of research and experimentation, especially for high-throughput gene expression measurements that can be used for diagnostics. Tsui et al. utilized the system as a tool for non-invasive prenatal diagnosis of the sex-linked hemophilia disease. Here, the BioMark system is used to perform digital PCR on DNA extracted from maternal plasma. The system served to automate the digital reaction setup by channeling nanoliter aliquots of PCR mixture into thousands of amplification chambers, resulting in a low-cost, high-throughput process [118]. Another example that utilizes the BioMark System was demonstrated by Yung et al. They used the system in the quantitative detection of two common epidermal growth factor receptor (EGFR) mutations in plasma and tumor tissues of nonsmall cell lung cancer patients. Use of the system enabled 9180 PCRs to be performed simultaneously at a nanoliter scale, whereby a single-mutant DNA molecule could be detected and quantities of mutant and wild-type sequences were determined [119]. Technologies like the Fluidigm BioMark System allow for low-cost, high-throughput single molecule amplifications that enable researchers to explore further and understand the basic fundamental biology that underlies complex diseases of the human body.

DNA microarray

DNA microarrays are popular microfluidic devices for genotyping [120–122]. The development of systems that can detect DNA is motivated by applications in the fields of gene profiling, disease diagnosing, and forensic analysis. DNA microarrays surfaced in the mid-1990s and have since created successful companies such as Affymetrix. Currently, efforts in DNA microarray technology are realizing fully automated systems that can perform every single step, from loading the analyte onto the microarray to automatically determining the presence of multiple genes of interest.

Working principle

DNA microarrays work on the principle of DNA hybridization. In this technique, a sequence that is complementary to a DNA sequence of interest is immobilized on a substrate (the chip). If the complementary sequence is present in the analyte, it will hybridize onto its complement located on the chip. Different methods are used to detect the hybridization event. Techniques include optical detection methods, usually involving fluorescently tagged DNA molecules, as well as surface plasmon resonance, colorimetric, and surface-enhanced Raman spectroscopy [123].

Implementation

DNA microarrays are usually made of glass, plastic, or silicon substrates. They contain hundreds of thousands of small oligonucleotides sequences. Oligonucleotides can be synthesized in situ or synthesized before being immobilized on a chip. The oligonucleotides are arranged spatially so that thousands of genes can be probed on a single chip. As a result, DNA microarrays have tremendous throughput because many different DNA probes can be placed on a single chip. Details of the implementation techniques were described in Chapter 2.

Applications

DNA microarrays, or gene chips, are used in DNA sequencing, gene expression, doxological research, and single nucleotide polymorphism (SNP) detection. An SNP is a DNA sequence variation with a single nucleotide (A, T, C, or G) different between different individuals (for example, TAAATAC and TAAGTAC). Genetic variations may cause differences in the susceptibility to disease. Some SNPs are used to predict an individual's response to certain drugs, and their susceptibility to toxins or diseases.

The massive parallelism of DNA arrays makes them attractive in applications that require screening large amounts of DNA for specific sequences. Although DNA microarrays have tremendous potential to be used as diagnostics devices in the clinic, most DNA microarrays are only used for research and development purposes due to lack of FDA approval. This is not surprising, as there are many technical, medical, and even marketing challenges to FDA approval. FDA-approved DNA microarray-based diagnostic devices include MammaPrint and AmpliChip. The MammaPrint is a test that assesses the risk of women having recurring breast

cancer after the initial tumor has been surgically removed or treated with chemotherapy. The test was developed by Agendia, and was approved by the FDA in 2007.

The AmpliChip CYP450 is the first FDA-approved (Class II device) DNA microarray-based test developed by Roche. It is a combination of the Affymetrix GeneChip technology and Roche's patented PCR amplification technology. It is used to screen for mutations in the CYP2D6 and CYP2C19 genes, which code for the production of CYP50 enzymes. These enzymes catalyze the oxidation of organic substances. They are responsible for the metabolism of about 25% of prescription drugs including anti-depressants, anti-psychotic, anti-epileptics, and beta-blockers [124]. A mutation to any of these genes will affect how effective prescription drugs are. Detecting mutations to the CYP2D6 and CYP2C19 genes provides information helpful to decide on a course of treatment.

Each AmpliChip CYP450 microarray has a 20 by 20 μm^2 square grid that contains 15,129 probes, with each probe having about 10^7 identical copies of a specific oligonucleotide [125]. The probes of the AmpliChip are synthesized using photodirected synthesis. Probes are grouped in sets of four, with each probe being different by a single nucleotide: A, C, G, or T. Only one of the four probes in a set is considered a "perfect" match; the other three are considered "mismatches." The probes on the AmpliChip CYP450 can differentiate between wild-type or mutant sequences.

Fig. 3.39 shows the protocol with the AmpliChip CYP450 microarray: First, patient DNA is purified from blood by PCR. The DNA is then fragmented by adding DNAase. The fragmented DNA is labeled with biotin. Next, the DNA is placed in

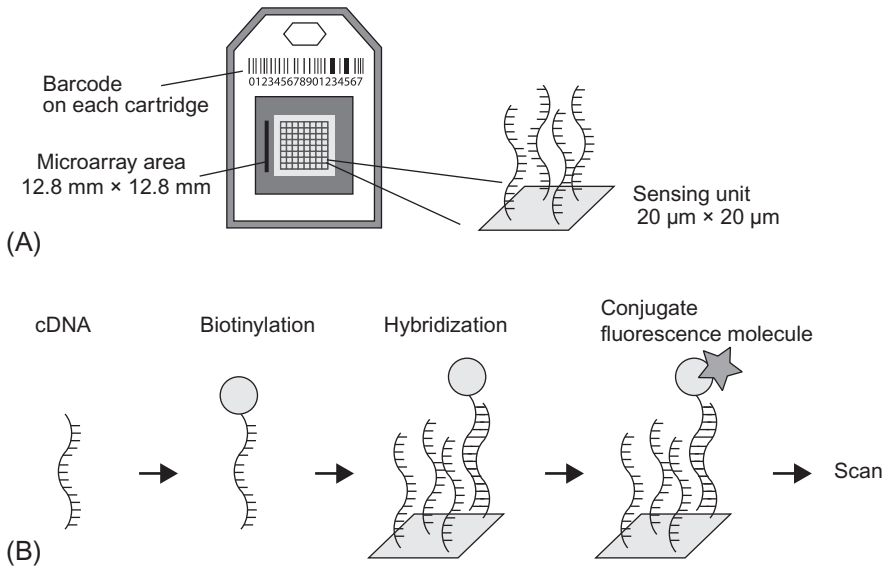

FIG. 3.39

(A) Design of Amplichip. (B) Process for detection.

contact with the microarray to allow patient DNA to hybridize with the DNA on the microarray. The unbound DNA is then washed away and the DNA that is bound is stained with streptavidin-conjugated fluorescent dye. The AmpliChip CYP450 is scanned using the Affymetrix GeneChip Microarray platform, which has a laser that excites the fluorescent dye. The amount of fluorescence is proportional to bond DNA on each probe of the microarray.

Microfluidic devices for DNA separation

Electrophoresis is a method to separate macromolecules such as DNA and protein by charge and size. It is very useful in separating DNA fragments and sorting, and is a critical step in DNA analysis and sequencing. *Gel electrophoresis* [126, 127] is a basic technique that separates analytes prepared in a porous gel medium. A gel is loaded with the analyte at one end. Electrodes are placed at opposite ends of the gel and the DNA fragments migrate towards the negative electrode. The rates of migration vary based on the size of fragments (Fig. 3.40). After a period of time, the potential difference is removed and the migrated DNA can be imaged. After electrophoresis, molecules can be stained for visualization. DNA may be visualized under ultraviolet light after the DNA is intercalated with ethidium bromide, a UV fluorescent agent. Proteins may be visualized using silver stain or Coomassie Brilliant Blue dye. Gel separations are used for characterization of DNA. The applications are numerous and can be used for hereditary analysis, DNA sequencing, immunology, and toxicology, to name a few.

Gel electrophoresis can be performed on samples on a microfluidic chip. Advantages of using microfluidic analysis systems include accuracy and performance on a

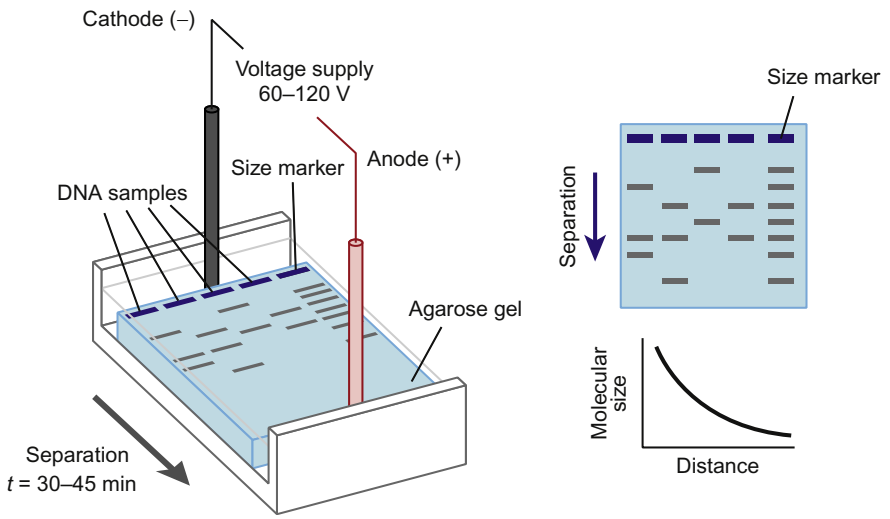

FIG. 3.40

Gel electrophoresis.

very small scale. In addition, many samples can be done in succession without having to reload samples, expediting DNA sequencing and analysis to provide instant lab results in a clinical environment [74, 78–81, 91–100].

Microfluidic electrophoresis

The conventional method of gel electrophoresis is an inexpensive method of analyzing proteins and DNA, but is very time consuming and requires skills for operation. Capillary electrophoresis on microfluidic chip devices [128, 129] can speed up and streamline the process. A microfluidic electrophoresis device requires a small sample to be placed in a reservoir. The entire process could be automated. Many samples can be processed in succession without having to reload samples. This can expedite the process of DNA sequencing and analysis, and make it more viable for instant lab results in a clinical environment.

Capillary electrophoresis separates macromolecules by size and electrical polarity. A microfluidic channel ranging from 5 to 200 μm in diameter is filled with a conducting buffer solution. A potential difference is applied to the ends of the capillary via electrodes placed in the sample and waste chambers (see Fig. 3.41). The difference in potential induces a current through the channel. Once current begins to flow, charged particles (i.e., DNA fragments) begin to flow. Since the rate of their flow is dependent on their charge, the DNA fragments are distributed by charge along the microchannel sometime later, in a way similar to a conventional gel electrophoresis.

Each well is connected to an electrode. A voltage is selectively applied to each pair of wells to perform sample injection and separation. The applied voltage ranges from 100 to 3000 V. Generally, about ~100 nL of sample is taken to be analyzed. Capillary electrophoresis is most often performed in glass micro-machined structures. The commonly used material is Corning 7740 Pyrex glass. Photolithographic techniques are employed to fabricate these devices. Channels of varying diameters can be etched into the glass with buffered HF.

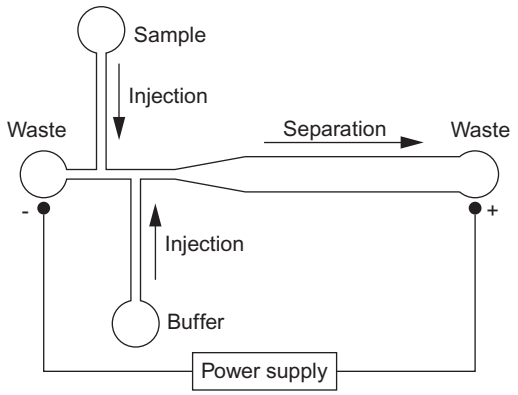

FIG. 3.41

Microchannel-based capillary electrophoresis.

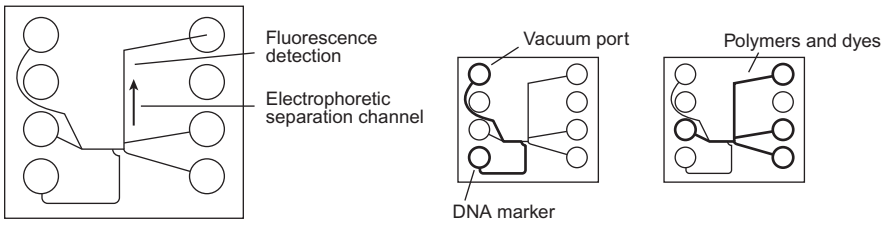

FIG. 3.42

Microchannel design used in PerkinElmer LabChip GX.

Commercial products

Some products currently exist on the market such as the LabChip GX from PerkinElmer. The LabChip GX bench top device streamlines the DNA analysis process and only requires the technician to place the sample in its reservoir. Fig. 3.42 shows the design of the LabChip electrophoresis system. The fluidic channel is about 50 μm wide and a few tens of micrometers deep. Fluorescent dye and sieving polymer are used in the separation procedure. An automated vacuum system pulls the sample into the separation channel with the proper mixture of buffer and then applies the voltage. A plug is created to prevent backflow from the separation channel. Voltage is then applied between the prepared sample chamber and the waste or end chamber to run the electrophoresis. Because very high voltages are used, electrophoresis only takes a few seconds. Longer times are not necessary because small amounts of sample are required. Once the separation is completed, the imaging step can now occur.

Agilent 2100 device is one of the most widely used commercial chip-based DNA analysis devices. These microfluidic chips are manufactured from PDMS using soft lithography. The system uses interchangeable chips that interface with a benchtop device that acts as the power supply for electrophoresis and also contains the optical detection system. The chip works largely in the same way as the PerkinElmer system [130–132]. Fig. 3.43 shows the overview of the Agilent LabChip, which is a cartridge including the microfluidic chip. The sample, buffer, and reagents are mixed, electrophoretically separated, and analyzed through fluorescence detection.

DNA sequencing

DNA sequencing is the process to determine the order of the four nucleotide bases—adenine (A), guanine (G), cytosine (C), and thymine (T)—in a DNA strand.

Sanger sequencing

Sanger sequencing, also known as the Sanger method, is widely used. This method has been modified in several ways since it was developed by Sanger and colleagues [133] in 1977. As of 2008, read-lengths and per-base accuracies achieved by the advanced Sanger method are as high as ∼1000 bp and 99.999%, respectively. It costs on the order of $0.50 per kilobase [134].

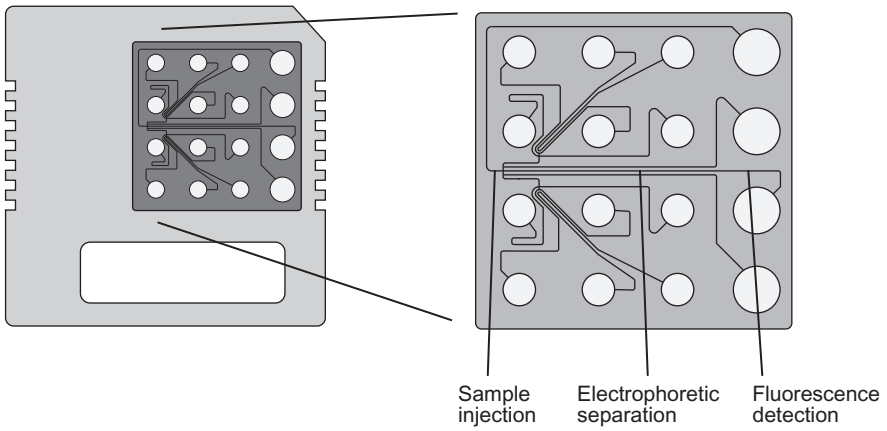

FIG. 3.43

Microchannel design in the Agilent LabChip.

DNA fragments are synthesized and terminated with one of the four nucleotide bases. The lengths of the fragments are measured by the following process:

The DNA sample is divided into four separate tubes containing deoxyribonucleotides (dNTPs) which are precursors to DNA synthesis and dideoxynucleotides (ddNTPs) which are chain-terminating inhibitors of DNA polymerase. Each tube contains all four of the standard deoxynucleotides (dATP, dGTP, dCTP, and dTTP) and one of the four dideoxynucleotides (ddATP, ddGTP, ddCTP, or ddTTP). The concentration of each ddNTP is about one-hundredth of those of the normal precursors (dNTPs).

During DNA synthesis, DNA polymerase adds nucleotides to the growing chain. A ddNTP is incorporated into the chain, replacing a normal nucleotide with a certain probability and creating a DNA fragment terminated at that point. As a result, each tube produces DNA fragments with different lengths, but always terminated at one of the four nucleotide bases (A,G,C,T) that corresponds to the ddNTP added in the tube (see the following example). The lengths of these DNA fragments can be found by sorting them with the gel electrophoresis or capillary electrophoresis technique.

Let us use an example sequence: GAAACATG. What we shall see from each tube is the lengths of the fragments that are synthesized, and we know at which base they are terminated.

Tube 1 (with ddATP: terminates at A).

?**A** (G**A** – AACATG)
??**A** (GA**A** – ACATG)
???**A** (GAA**A** – CATG)
?????**A** (GAAAC**A** – TG)

Tube 2 (with ddGTP: terminates at G).

G (**G** – AACATG)
???????**G** (GAAACAT**G**)

Tube 3 (with ddCTP: terminates at C).

????**C** (GAAA**C**-ATG)

Tube 4 (with ddTTP: terminates at T).

??????**T** (GAAACA**T**-G)

When we sort these fragments based on the lengths:

G
?A
??A
???A
????C
?????A
??????T
???????G

Now we find that the original DNA sequence was GAAACATG.

Microfluidic systems for Sanger sequencing

One approach for microfluidic DNA sequencing is miniaturizing Sanger sequencing. Mathies et al. developed a microfluidic device integrating all three Sanger sequencing steps: Sanger extension, purification, and electrophoretic analysis [135]. Fig. 3.44 illustrates a flow chart of conventional DNA sequencing. DNA is extracted from cultured cells and amplified. Sanger extension is then performed and purified to be analyzed on a capillary array electrophoresis (CAE) sequencer. Fig. 3.44B shows microfabricated sequencing lab on a chip. Each step of the conventional protocol is miniaturized into a 15 cm-diameter microdevice, where 96 lanes are integrated into 48 doublet structures.

The same group performed complete Sanger sequencing from a 1 fmol DNA template. Up to 556 continuous bases were sequenced with 99% accuracy [136].

Nanopore-based sequencing

A miniaturization technique very different from conventional Sanger sequencing is nanopore-based sequencing [137]. It is based on translocation of a DNA molecule through a nanometer-sized pore that is large only enough for a single strand of RNA or DNA. Types of pores under investigation are categorized into two types: protein pores and solid-state pores. Kasianowics et al. used a 2.6-nm diameter ion channel in a lipid bilayer membrane. The membrane was formed across a ~100 μm diameter orifice in a 25-μm thick Teflon partition that separates two buffer-filled compartments. The passage of each polynucleotide molecule was measured as a transient decrease of ionic current whose duration is proportional to the length of the molecule [138]. Oxford Nanopore Technologies has developed a portable system called the MiniION, which utilizes consumable protein flow cells. The device can generate 10–20 Gb of sequence data, and research shows that by

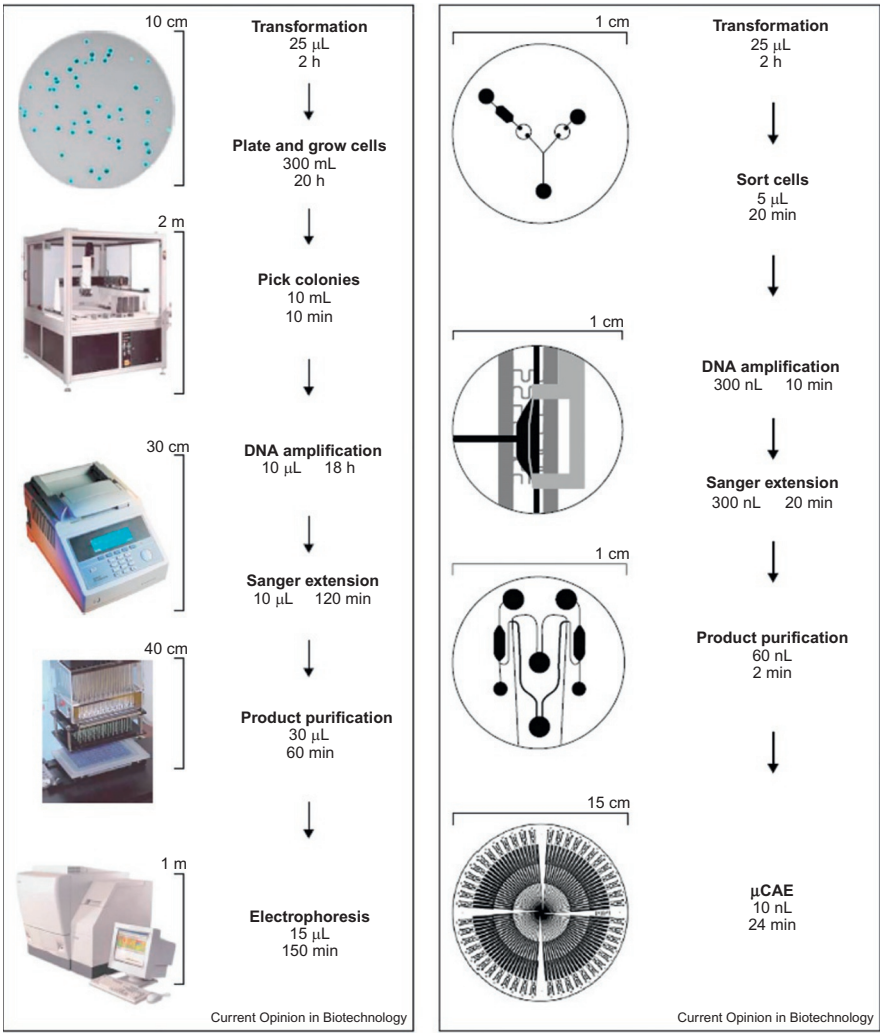

FIG. 3.44

(A) A flow chart for conventional DNA sequencing. (B) Microfabricated DNA sequencing microdevice.

Both reprinted from B.M. Paegel, R.G. Blazej, R.A. Mathies, Microfluidic devices for DNA sequencing: sample preparation and electrophoretic analysis, Curr. Opin. Biotechnol. 14 (2003) 42–50, with permission from Elsevier.

optimizing computational parameters, the portable sequencer could be used to sequence, assemble, and provisionally analyze structural variants and detect epigenetic marks in the human genome [139].

Development of solid-state nanopores is a topic of ongoing studies. Fig. 3.45 illustrates a solid state nanopore. Fig. 3.45 illustrates schematics of the experiment.

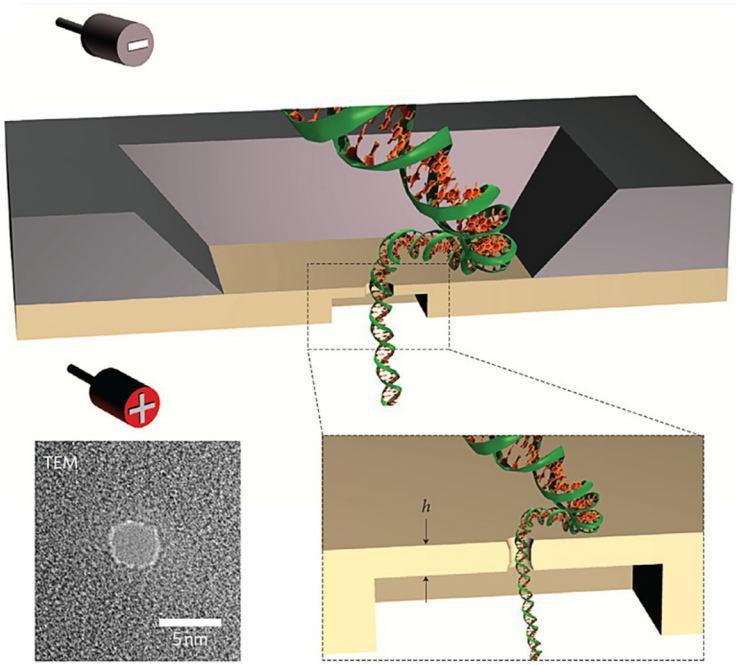

FIG. 3.45

Illustration of DNA molecule translocating through a solid-state nanopore and a TEM micrograph of a 4-nm silicon nitride nanopore in a 6-nm thick local membrane.

Reprinted by permission of Nature: M. Wanunu, T. Dadosh, V. Ray, J. Jin, L. McReynolds, M. Drndić, Rapid electronic detection of probe-specific microRNAs using thin nanopore sensors. Nat. Nanotechnol. 5 (2010), 807, Copyright 2010.

Two isolated reservoirs are insulated by a silicon nitride membrane containing a single nanopore. An ionic current through the nanopore is induced by a bias voltage applied between the two reservoirs. While DNA molecules pass through the nanopore due to their negative charge, nanopore current is recorded to assess the molecule's interaction with the nanopore. The nanopore shown in Fig. 3.45 was fabricated through a membrane locally thinned to 6 nm [140].

When a molecule passes through a nanopore, the ion current is reduced because the nanopore is partially blocked by the translocating molecule. One hypothesis for future nanopore-based DNA sequencing is that the sequence of ionic current reduction may reflect that of bases in the polynucleotide molecule [137]. Manrao et al. demonstrated the ability to resolve changes in current that correspond to a known DNA sequence [141]. They used a mutated form of the protein pore Mycobacterium smegmatis porin A (MspA) with phi29 DNA polymerase (DNAP). Phi29 DNAP controls the rate of DNA passage by acting like a motor to pull a single-stranded template through MspA as it synthesizes DNA (Fig. 3.46A). The authors recorded

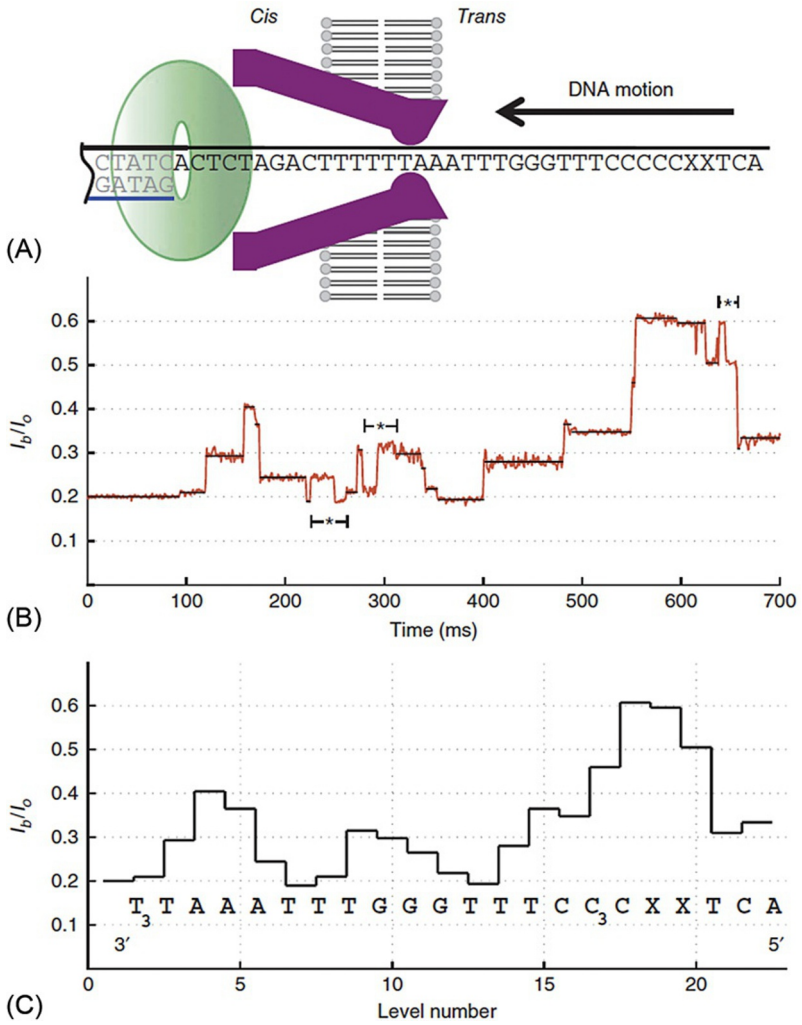

FIG. 3.46

Nanopore-based single-nucleotide resolution sequencing.

Reprinted by permission of Nature: E.A. Manrao, I.M. Derrington, A.H. Laszlo, K.W. Langford, M.K. Hopper, N. Gillgren, et al., Reading DNA at single-nucleotide resolution with a mutant MspA nanopore and phi29 DNA polymerase, Nat. Biotechnol. 30 (2012) 349–353, Copyright 2012.

current sequences that match the known sequences using DNA sequences with ~50-nucleotide-long readable regions (Fig. 3.46B and C).

Before solid-state nanopores can be more widely adopted, there are many hurdles to overcome. Issues include the creation of a large-scale, repeatable, and low-cost fabrication, controllable speed through the pore, and increased sensitivity of the electrical output [142].

PROBLEMS

1. Diffusion
   (1) If a molecule has diffused 10 nm in 1 s, how far does it travel in 4 s?
   (2) We measured that hemoglobin (diffusion coefficient $D = 7 \times 10^{-7}$ cm^2/s) in water takes 1 million seconds to diffuse 1 cm. A student designed a microfluidic channel with the width of 10 μm to mimic such a diffusion experiment at small scale.
   - How long does it take for hemoglobin to diffuse across such microfluidic channel?
   - Based on your calculation in (b1), is it a good idea to design microfluidic diffusion-based mixers?
2. Spindle viscometer
   (1) A liquid is contained between a cylindrical spindle and a cylindrical container. The height and the radius of the spindle are 15 and 10 mm, respectively. The gap between the spindle and the container is 1 mm. Because of the air trapped at the bottom of the spindle, viscous drag arises only on the sidewall of the spindle. If the torque of $T = 6.2 \times 10^{-6}$ N·m is needed to rotate a spindle at 50 rpm, what is the viscosity of the liquid?

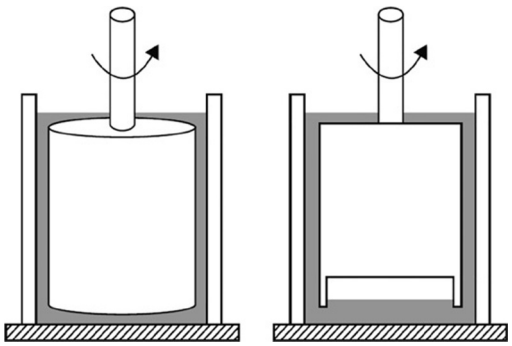

   (2) The figure shows another type of viscometer where a liquid is contained between a cone-shaped spindle with an angle of 3° and a stationary substrate. The radius of the spindle is 20 mm. Calculate the torque needed to rotate the spindle at a rotational speed of 20 RPM when the viscosity of the liquid is 30 cP.

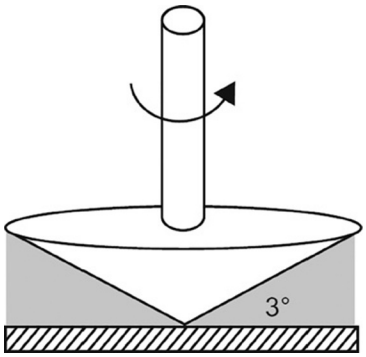

3. Hagen-Poiseuille equation

A micro-capillary tubing can be used as a simple viscometer. The viscosity can be found from the flow rate, pressure drop, and the tube geometry. Here is a measurement of a certain liquid in a capillary viscometer. Find the viscosity of the liquid.

Flow rate: 880 mm^3 /s
Tube diameter: 500 μm
Tube length: 100 mm
Pressure drop: 0.1 MPa

4. Reynolds number

An accepted transition Reynolds number for flow in a circular pipe is $Re = 2300$. For flow through a 100-μm diameter pipe, at what velocity will the transition occur at 20°C for (a) airflow and (b) water flow? Assume the kinetic viscosity of air at 20°C is 1.5×10^{-5} m^2/s, and for water is 1.0×10^{-6} m^2/s.

5. Reynolds number

Estimate the Reynolds numbers associated with a honeybee, hummingbird, condor, and airplane. Use the information in the following table. The chord length is usually taken as the characteristic length to find the Reynolds number of a wing. The kinematic viscosity of air is 1×10^{-5} m^2/s. Discuss the differences in the way they fly.

	Honeybee	**Hummingbird**	**Condor**	**Airplane**
Wing chord length	5 mm	3 cm	30 cm	3 m
Fly parameters	Wing flaps: 200 times/s	Wing flaps: 50 times/s	Velocity: 50 km/h	*V*elocity: 1000 km/h
Reynolds numbers				

6. Reynolds number

The photograph is a microscopic image of a cancer spheroid (a spherical cluster of cancer cells). This spheroid is located in a microfluidic channel, and the medium is flowing at an average velocity of U. Consider the spheroid as a 300-μm sphere and find the Reynolds number. When we find the Reynolds number of a sphere in a fluid, the diameter is generally used as the characteristic length L.

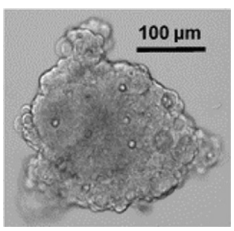

Average velocity: $U = 1$ mm/s
Medium viscosity: $\mu = 1$ cP
Medium density: $\rho = 1$ g/cm^3

7. Laminar flow

Let us consider a flow between two parallel plates as shown in the following figure. The viscosity of the fluid is μ, the gap between the two plate is H, and the average flow velocity is U.

(1) Form a differential equation of motion for a thin layer from y to $y + \Delta y$.

(2) Show that the same equation as (1) can be derived from the Navier-Stokes equation.

(3) Find the velocity profile $u_x(y)$ by solving the differential equation formed in (1).

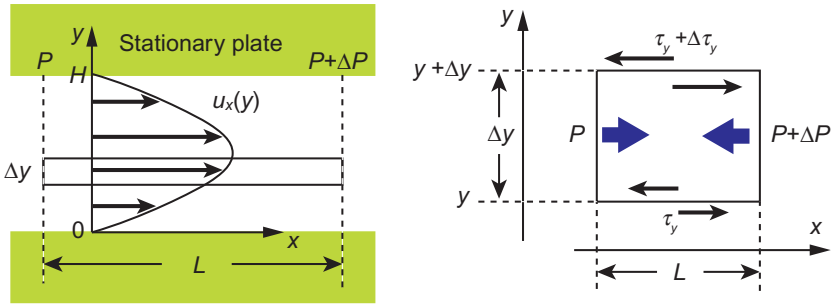

8. Laminar flow

There is a flat microchannel with dimensions of width $w = 5$ mm, thickness $t = 0.5$ mm, and length $l = 20$ mm. Assume the flow is laminar and uniform in the directions of the width and the length. A liquid flows in the channel at a flow rate of $Q = 2.5$ mL/h. Find how the velocity profile in z-direction follows a simple parabola defined by the flow rate Q.

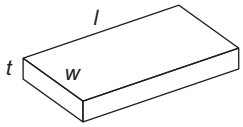

9. Diffusion in microchannel

Consider a y-channel where two flows (flow1 and flow2) of a buffer solution meet at the intersection. Flow2 contains particles with the diffusion constant of $D = 5 \times 10^{-14}$ m^2/s. The average velocity of the main flow is $U = 0.8$ mm/s.

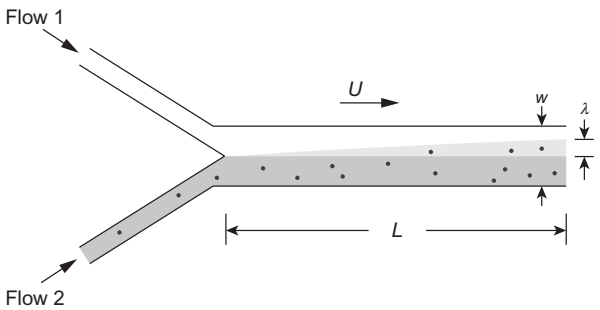

(1) When L = 22 mm, how long is the depth of diffusion λ at the right end?

(2) We want to use this y-channel as a passive mixer. The diffusion from flow2 has to reach the other side of the channel. Find the minimum length L. Use the width of the channel $w = 100$ μm.

10. Microfluidic pump

A microdevice engineer is designing a passive microfluidic "pump" to manipulate blood droplets. As shown in the figure, two droplets are deposited at each end of a microfluidic channel, with the larger droplet on the left end. The channel is filled with blood. Without using any external force, in which direction would you think the blood is going to move?

(a) From left to right, the larger droplet will disappear and the small droplet will grow bigger.

(b) From right to left, the small droplet will disappear and the larger droplet will grow bigger.

(c) No moving action involved; the pump does not work.

Choose from (a), (b), and (c), and justify your choice.

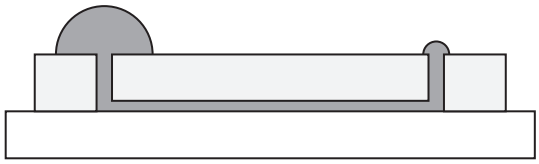

11. Hagen-Poiseuille equation

A liquid with the viscosity μ is flowing in a circular microchannel with the radius of r and the length of L at a flow rate of Q pumped with a pressured of ΔP. The flow can be treated as laminar.

You now need to design another microchannel for a liquid with the viscosity of 2 μ. You have to use the same pumping pressure ΔP to keep the same flow rate Q.

(1) If you can only change the length, what will be the length?

(2) If you can only change the radius, what will be the radius?

12. Hagen-Poiseuille equation

You apply pressure of ΔP to Tube 1 (inside radius $r_1 = 0.004$ m, length $L_1 = 0.1$ m) and obtain the flow rate of Q_1. Tube 2 is another tube (inside radius r_2, length $L_2 = 1$ m), which is longer than Tube 1. You obtain a flow rate of Q_2 at the same applied pressure ΔP.

(1) If the radii of the two tubes are the same ($r_2 = r_1$), describe the relationship between Q_1 and Q_2.

(2) In order to obtain the same flow rates for Tube 1 and Tube 2 ($Q_1 = Q_2$), how large should the radius of Tube 2 ($= r_2$) be?

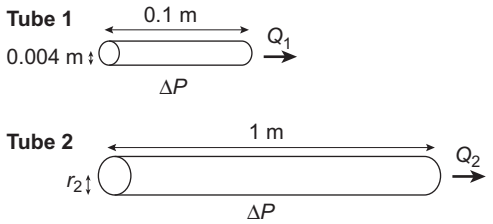

13. Hagen-Poiseuille equation

(1) Describe the pressure drop ΔP along the micro channel shown in the left-hand figure. You may use average velocity U, channel radius R, viscosity η, and flow rate Q.

(2) A flow introduced from the inlet is divided into two in a micro fluidic system shown in the right-hand figure. Calculate output flow rates Q_1 and Q_2. You may use incoming flow rate Q, radii R_1 and R_2 and channel lengths L_1 and L_2. Neglect the pressure drop at the connection. The fluid pressures at the two outlets are the same.

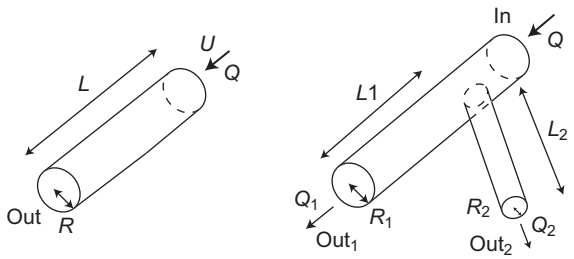

14. Immunomagnetic separation

The following figure shows a top view of a typical implementation of immunomagnetic cells separation, where a test tube with a diameter of 10 mm is surrounded by four magnets. The contour map shows simulated magnetic field intensities. The magnitude of the field changes from $T = 0$ at the center to $T = 0.03$ at the wall.

(1) Estimate the value of $\partial B^2/\partial r$ in the tube. Assume that the magnetic field intensity B changes linearly along the radial direction.

(2) Contained in the tube is blood that includes ~200 cancer cells labeled with magnetic nanoparticles. Calculate how long it takes to collect all the labeled cells to the side wall. Use the radius of the cells $R_C = 7.5$ μm, the effective magnetic volumetric susceptibility of the cell $\Delta\chi_C = 3 \times 10^{-3}$, the magnetic permeability of vacuum $\mu_0 = 4\pi \times 10^{-7}\,\mathrm{T\,m\,A^{-1}}$, and blood viscosity $\eta_B = 7.5 \times 10^{-3}\,\mathrm{kg\,m^{-1}\,s^{-1}}$.

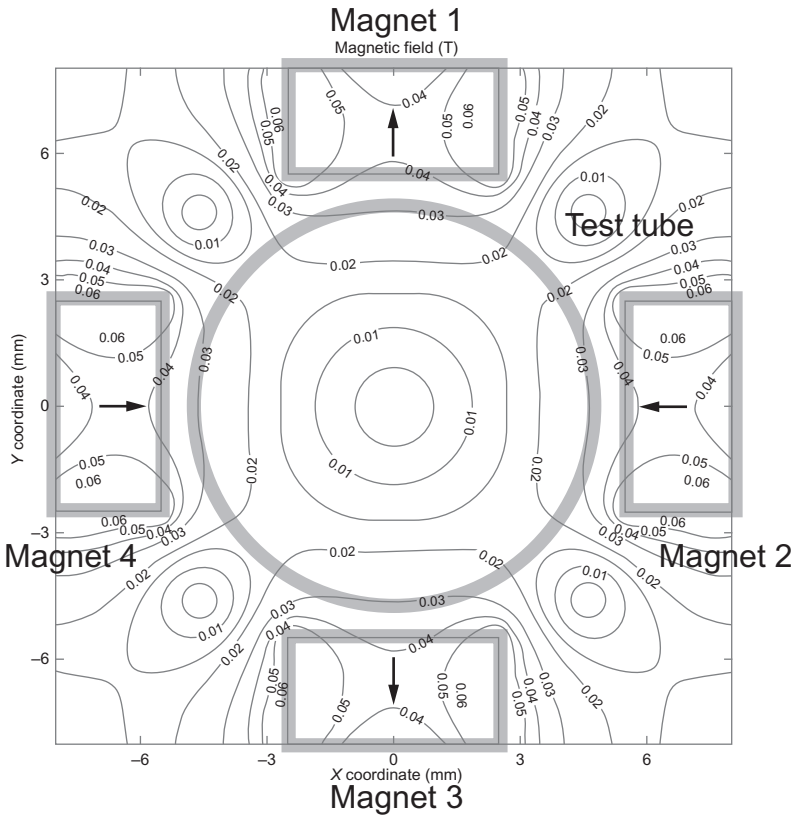

15. Circulating tumor cells

(1) Name three benefits of a system that can detect cancer cells from blood.

(2) Name three difficulties in the commercialization of such a system.

(3) Name six methods of separating cancer cells from blood. Which method do you think is the most promising method? Explain why.

16. Gel electrophoresis

In gel electrophoresis, the amount of electrical charge is the (larger, smaller, same) for the longer DNA fragment. The viscous force acting on a DNA fragment is the (larger, smaller, same) for the longer DNA fragment. The rates of migration are the (larger, smaller, same) for the longer DNA fragment.

17. PCR

Design a forward and reverse primer suitable for amplifying the underlined segment of "GACCTCCCAGGCCAGTGCAGTCGGGCC." In a practical case, primers are 10–25 bp long and the amplicon is 500 bp long; however, for this exercise, design primers are 5 bp long.

18. PCR

We have prepared cDNAs from 10 cells and 10,000 cells. If we want to obtain the same amount of amplified DNA using PCR, what is the expected difference between the cycle times for the two samples?

19. Fluidic focusing, Reynolds number

You are designing a microfluidic flow cytometer based on a rectangular microchannel as illustrated in Fig. 3.16(A). In order to have proper fluidic focusing of particles, the sheath flow has to be laminar. When the cross-sectional dimensions of the sheath flow are $w = 500$ μm and $h = 300$ μm, how much is the maximum allowable flow rate? Use the viscosity of the media: 1 cP.

REFERENCES

[1] B. Eckhardt, Introduction. Turbulence transition in pipe flow: 125th anniversary of the publication of Reynolds' paper, Philos. Trans. R. Soc. A Math. Phys. Eng. Sci. 367 (2009) 449–455.

[1a] K. Schmidt-Nielsen, Scaling: Why is Animal Size so Important? Cambridge University Press, 1984.

[2] E.M. Purcell, Life at low Reynolds number, Am. J. Phys. 45 (1977) 3–11.

[3] H.A. Stone, A.D. Stroock, A. Ajdari, Engineering flows in small devices: microfluidics toward a lab-on-a-chip, Annu. Rev. Fluid Mech. 36 (2004) 381–411.

[4] P.S. Dittrich, A. Manz, Lab-on-a-chip: microfluidics in drug discovery, Nat. Rev. Drug Discov. 5 (2006) 210–218.

[5] H. Becker, C. Gärtner, Polymer microfabrication methods for microfluidic analytical applications, Electrophoresis 21 (2000) 12–26.

[6] D.J. Beebe, G.A. Mensing, G.M. Walker, Physics and applications of microfluidics in biology, Annu. Rev. Biomed. Eng. 4 (2002) 261–286.

[7] R. Konrad, A. Griebel, W. Dörner, H. Löwe, Towards disposable lab-on-a-chip: poly(methylmethacrylate) microchip electrophoresis device with electrochemical detection, Electrophoresis 23 (2002) 596–601.

[8] C.H. Ahn, J.-W. Choi, G. Beaucage, J.H. Nevin, J.-B. Lee, A. Puntambekar, et al., Disposable smart lab on a chip for point-of-care clinical diagnostics, Proc. IEEE 92 (2004) 154–173.

[9] C.D. Chin, V. Linder, S.K. Sia, Lab-on-a-chip devices for global health: past studies and future opportunities, Lab Chip 7 (2007) 41–57.

[10] G.M. Whitesides, The origins and the future of microfluidics, Nature 442 (2006) 368–373.

[11] J.R. Anderson, D.T. Chiu, H. Wu, O.J. Schueller, G.M. Whitesides, Fabrication of microfluidic systems in poly(dimethylsiloxane), Electrophoresis 21 (2000) 27–40.

[12] H. Lorenz, M. Despont, N. Fahrni, N. LaBianca, P. Renaud, P. Vettiger, SU-8: a low-cost negative resist for MEMS, J. Micromech. Microeng. 7 (1997) 121.

[13] J. Haneveld, H. Jansen, E. Berenschot, N. Tas, M. Elwenspoek, Wet anisotropic etching for fluidic 1D nanochannels, J. Micromech. Microeng. 13 (2003) S62.

[14] A. Nilsson, F. Petersson, H. Jönsson, T. Laurell, Acoustic control of suspended particles in micro fluidic chips, Lab Chip 4 (2004) 131–135.
[15] L. Jiang, J. Mikkelsen, J.-M. Koo, D. Huber, S. Yao, L. Zhang, et al., Closed-loop electroosmotic microchannel cooling system for VLSI circuits, IEEE Trans. Component Pack. Technol. 25 (2002) 347–355.
[16] D. Di Carlo, K.-H. Jeong, L.P. Lee, Reagentless mechanical cell lysis by nanoscale barbs in microchannels for sample preparation, Lab Chip 3 (2003) 287–291.
[17] H. Becker, U. Heim, Hot embossing as a method for the fabrication of polymer high aspect ratio structures, Sens. Actuator A Phys. 83 (2000) 130–135.
[18] R.M. McCormick, R.J. Nelson, M.G. Alonso-Amigo, D.J. Benvegnu, H.H. Hooper, Microchannel electrophoretic separations of DNA in injection-molded plastic substrates, Anal. Chem. 69 (1997) 2626–2630.
[19] A. Kaiser, C.J. Klok, J.J. Socha, W.-K. Lee, M.C. Quinlan, J.F. Harrison, Increase in tracheal investment with beetle size supports hypothesis of oxygen limitation on insect gigantism, Proc. Natl. Acad. Sci. 104 (2007) 13198–13203.
[20] N.-T. Nguyen, Z. Wu, Micromixers—a review, J. Micromech. Microeng. 15 (2005) R1.
[21] R.H. Liu, M.A. Stremler, K.V. Sharp, M.G. Olsen, J.G. Santiago, R.J. Adrian, et al., Passive mixing in a three-dimensional serpentine microchannel, J. Microelectromech. Syst. 9 (2000) 190–197.
[22] A.D. Stroock, S.K.W. Dertinger, A. Ajdari, I. Mezić, H.A. Stone, G.M. Whitesides, Chaotic mixer for microchannels, Science 295 (2002) 647–651.
[23] H. Wang, P. Iovenitti, E. Harvey, S. Masood, Optimizing layout of obstacles for enhanced mixing in microchannels, Smart Mater. Struct. 11 (2002) 662.
[24] W.C. Chang, L.P. Lee, D. Liepmann, Biomimetic technique for adhesion-based collection and separation of cells in a microfluidic channel, Lab Chip 5 (2005) 64–73.
[25] S. Nagrath, L.V. Sequist, S. Maheswaran, D.W. Bell, D. Irimia, L. Ulkus, et al., Isolation of rare circulating tumour cells in cancer patients by microchip technology, Nature 450 (2007) 1235–1239.
[26] H. Song, J.D. Tice, R.F. Ismagilov, A microfluidic system for controlling reaction networks in time, Angew. Chem. 115 (2003) 792–796.
[27] T.M. Squires, S.R. Quake, Microfluidics: fluid physics at the nanoliter scale, Rev. Mod. Phys. 77 (2005) 977.
[28] J.P. Brody, P. Yager, Diffusion-based extraction in a microfabricated device, Sens. Actuator A Phys. 58 (1997) 13–18.
[29] H.M. Shapiro, Practical Flow Cytometry, Wiley-Liss, 2005.
[30] H.M. Davey, D.B. Kell, Flow cytometry and cell sorting of heterogeneous microbial populations: the importance of single-cell analyses, Microbiol. Rev. 60 (1996) 641–696.
[31] A. Krishan, H. Krishnamurthy, S. Totey, Applications of Flow Cytometry in Stem Cell Research and Tissue Regeneration, Wiley-Blackwell, 2011.
[32] A.Y. Fu, C. Spence, A. Scherer, F.H. Arnold, S.R. Quake, A microfabricated fluorescence-activated cell sorter, Nat. Biotechnol. 17 (1999) 1109–1111.
[33] A. Wolff, I.R. Perch-Nielsen, U. Larsen, P. Friis, G. Goranovic, C.R. Poulsen, et al., Integrating advanced functionality in a microfabricated high-throughput fluorescent-activated cell sorter, Lab Chip 3 (2003) 22–27.
[34] M.M. Wang, E. Tu, D.E. Raymond, J.M. Yang, H. Zhang, N. Hagen, et al., Microfluidic sorting of mammalian cells by optical force switching, Nat. Biotechnol. 23 (2004) 83–87.

[35] X. Mao, S.-C.S. Lin, C. Dong, T.J. Huang, Single-layer planar on-chip flow cytometer using microfluidic drifting based three-dimensional (3D) hydrodynamic focusing, Lab Chip 9 (2009) 1583–1589.
[36] W. Lee, D. Kwon, W. Choi, G.Y. Jung, A.K. Au, A. Folch, et al., 3D-printed microfluidic device for the detection of pathogenic bacteria using size-based separation in helical channel with trapezoid cross-section, Sci. Rep. 5 (2015) 7717.
[37] U.A. Gurkan, T. Anand, H. Tas, D. Elkan, A. Akay, H.O. Keles, et al., Controlled viable release of selectively captured label-free cells in microchannels, Lab Chip 11 (2011) 3979–3989.
[38] A.A. Adams, P.I. Okagbare, J. Feng, M.L. Hupert, D. Patterson, J. Göttert, et al., Highly efficient circulating tumor cell isolation from whole blood and label-free enumeration using polymer-based microfluidics with an integrated conductivity sensor, J. Am. Chem. Soc. 130 (2008) 8633–8641.
[39] S.L. Stott, C.-H. Hsu, D.I. Tsukrov, M. Yu, D.T. Miyamoto, B.A. Waltman, et al., Isolation of circulating tumor cells using a microvortex-generating herringbone-chip, Proc. Natl. Acad. Sci. 107 (2010) 18392–18397.
[40] S. Moon, U.A. Gurkan, J. Blander, W.W. Fawzi, S. Aboud, F. Mugusi, et al., Enumeration of CD4+ T-cells using a portable microchip count platform in Tanzanian HIV-infected patients, PLoS One 6 (2011), e21409.
[41] C.D. Chin, T. Laksanasopin, Y.K. Cheung, D. Steinmiller, V. Linder, H. Parsa, et al., Microfluidics-based diagnostics of infectious diseases in the developing world, Nat. Med. 17 (2011) 1015–1019.
[42] S.K. Sia, V. Linder, B.A. Parviz, A. Siegel, G.M. Whitesides, An integrated approach to a portable and low-cost immunoassay for resource-poor settings, Angew. Chem. Int. Ed. 43 (2004) 498–502.
[43] S. Wang, H. Wang, J. Jiao, K.J. Chen, G.E. Owens, K.i. Kamei, et al., Three-dimensional nanostructured substrates toward efficient capture of circulating tumor cells, Angew. Chem. 121 (2009) 9132–9135.
[44] Y. Xu, J.A. Phillips, J. Yan, Q. Li, Z.H. Fan, W. Tan, Aptamer-based microfluidic device for enrichment, sorting, and detection of multiple cancer cells, Anal. Chem. 81 (2009) 7436–7442.
[45] D.W. Inglis, R. Riehn, R. Austin, J. Sturm, Continuous microfluidic immunomagnetic cell separation, Appl. Phys. Lett. 85 (2004) 5093–5095.
[46] P.A. Liberti, C.G. Rao, L.W.M.M. Terstappen, Optimization of ferrofluids and protocols for the enrichment of breast tumor cells in blood, J. Magn. Magn. Mater. 225 (2001) 301–307.
[47] A.A.H. Talasaz, A.A. Powell, D.E. Huber, J.G. Berbee, K.H. Roh, W. Yu, et al., Isolating highly enriched populations of circulating epithelial cells and other rare cells from blood using a magnetic sweeper device, Proc. Natl. Acad. Sci. 106 (2009) 3970–3975.
[48] M. Radisic, R.K. Iyer, S.K. Murthy, Micro- and nanotechnology in cell separation, Int. J. Nanomed. 1 (2006) 3.
[49] S. Miltenyi, W. Müller, W. Weichel, A. Radbruch, High gradient magnetic cell separation with MACS, Cytometry 11 (1990) 231–238.
[50] P.A. Taylor, A. Panoskaltsis-Mortari, J.M. Swedin, P.J. Lucas, R.E. Gress, B.L. Levine, et al., L-Selectinhi but not the L-selectinlo CD4+ 25+ T-regulatory cells are potent inhibitors of GVHD and BM graft rejection, Blood 104 (2004) 3804–3812.

[51] T.T. Hansel, I.J.M. De Vries, T. Iff, S. Rihs, M. Wandzilak, S. Betz, et al., An improved immunomagnetic procedure for the isolation of highly purified human blood eosinophils, J. Immunol. Methods 145 (1991) 105–110.
[52] X. Zhao, E. Deak, K. Soderberg, M. Linehan, D. Spezzano, J. Zhu, et al., Vaginal submucosal dendritic cells, but not Langerhans cells, induce protective Th1 responses to herpes simplex virus-2, J. Exp. Med. 197 (2003) 153–162.
[53] M. Bauer, V. Redecke, J.W. Ellwart, B. Scherer, J.P. Kremer, H. Wagner, et al., Bacterial CpG-DNA triggers activation and maturation of human CD11c-, CD123+ dendritic cells, J. Immunol. 166 (2001) 5000–5007.
[54] M.A. Burchill, J. Yang, C. Vogtenhuber, B.R. Blazar, M.A. Farrar, IL-2 receptor β-dependent STAT5 activation is required for the development of Foxp3+ regulatory T cells, J. Immunol. 178 (2007) 280–290.
[55] M.C. Miller, G.V. Doyle, L.W.M.M. Terstappen, Significance of circulating tumor cells detected by the CellSearch system in patients with metastatic breast colorectal and prostate cancer, J. Oncol. 2010 (2009).
[56] P. Paterlini-Brechot, N.L. Benali, Circulating tumor cells (CTC) detection: clinical impact and future directions, Cancer Lett. 253 (2007) 180–204.
[57] B. Mostert, S. Sleijfer, J.A. Foekens, J.W. Gratama, Circulating tumor cells (CTCs): detection methods and their clinical relevance in breast cancer, Cancer Treat. Rev. 35 (2009) 463–474.
[58] W.J. Allard, J. Matera, M.C. Miller, M. Repollet, M.C. Connelly, C. Rao, et al., Tumor cells circulate in the peripheral blood of all major carcinomas but not in healthy subjects or patients with nonmalignant diseases, Clin. Cancer Res. 10 (2004) 6897–6904.
[59] T. Fehm, A. Sagalowsky, E. Clifford, P. Beitsch, H. Saboorian, D. Euhus, et al., Cytogenetic evidence that circulating epithelial cells in patients with carcinoma are malignant, Clin. Cancer Res. 8 (2002) 2073–2084.
[60] G.T. Budd, M. Cristofanilli, M.J. Ellis, A. Stopeck, E. Borden, M.C. Miller, et al., Circulating tumor cells versus imaging—predicting overall survival in metastatic breast cancer, Clin. Cancer Res. 12 (2006) 6403–6409.
[61] T.H. Boyer, The force on a magnetic dipole, Am. J. Phys. 56 (1988) 688.
[62] Q.A. Pankhurst, J. Connolly, S. Jones, J. Dobson, Applications of magnetic nanoparticles in biomedicine, J. Phys. D. Appl. Phys. 36 (2003) R167.
[63] N. Xia, T.P. Hunt, B.T. Mayers, E. Alsberg, G.M. Whitesides, R.M. Westervelt, et al., Combined microfluidic-micromagnetic separation of living cells in continuous flow, Biomed. Microdevices 8 (2006) 299–308.
[64] C.W. Yung, J. Fiering, A.J. Mueller, D.E. Ingber, Micromagnetic-microfluidic blood cleansing device, Lab Chip 9 (2009) 1171–1177.
[65] V.I. Furdui, J.K. Kariuki, D.J. Harrison, Microfabricated electrolysis pump system for isolating rare cells in blood, J. Micromech. Microeng. 13 (2003) S164.
[66] S. Karl, M. David, L. Moore, B.T. Grimberg, P. Michon, I. Mueller, et al., Enhanced detection of gametocytes by magnetic deposition microscopy predicts higher potential for *Plasmodium falciparum* transmission, Malar. J. 7 (2008) 66.
[67] B. Fang, M. Zborowski, L.R. Moore, Detection of rare MCF-7 breast carcinoma cells from mixtures of human peripheral leukocytes by magnetic deposition analysis, Cytometry 36 (1999) 294–302.
[68] K. Hoshino, Y.Y. Huang, N. Lane, M. Huebschman, J.W. Uhr, E.P. Frenkel, et al., Microchip-based immunomagnetic detection of circulating tumor cells, Lab Chip 11 (2011) 3449–3457.

[69] K. Hoshino, P. Chen, Y.Y. Huang, X. Zhang, Computational analysis of microfluidic immunomagnetic rare cell separation from a particulate blood flow, Anal. Chem. 84 (2012) 4292–4299.
[70] Y. Huang, K. Hoshino, P. Chen, C. Wu, N. Lane, M. Huebschman, et al., Immunomagnetic nanoscreening of circulating tumor cells with a motion controlled microfluidic system, Biomed. Microdevices (2012) 1–9.
[71] J.W. Choi, K.W. Oh, A. Han, C.A. Wijayawardhana, C. Lannes, S. Bhansali, et al., Development and characterization of microfluidic devices and systems for magnetic bead-based biochemical detection, Biomed. Microdevices 3 (2001) 191–200.
[72] N. Pamme, Magnetism and microfluidics, Lab Chip 6 (2005) 24–38.
[73] F.F. Becker, X.B. Wang, Y. Huang, R. Pethig, J. Vykoukal, P. Gascoyne, Separation of human breast cancer cells from blood by differential dielectric affinity, Proc. Natl. Acad. Sci. 92 (1995) 860–864.
[74] F. Yang, X. Yang, H. Jiang, P. Bulkhaults, P. Wood, W. Hrushesky, et al., Dielectrophoretic separation of colorectal cancer cells, Biomicrofluidics 4 (2010), 013204.
[75] F. Petersson, L. Åberg, A.M. Swärd-Nilsson, T. Laurell, Free flow acoustophoresis: microfluidic-based mode of particle and cell separation, Anal. Chem. 79 (2007) 5117–5123.
[76] A. Lenshof, A. Ahmad-Tajudin, K. Järås, A.M. Swärd-Nilsson, L. Åberg, G. Marko-Varga, et al., Acoustic whole blood plasmapheresis chip for prostate specific antigen microarray diagnostics, Anal. Chem. 81 (2009) 6030–6037.
[77] A.A.S. Bhagat, H. Bow, H.W. Hou, S.J. Tan, J. Han, C.T. Lim, Microfluidics for cell separation, Med. Biol. Eng. Comput. 48 (2010) 999–1014.
[78] J. Hultström, O. Manneberg, K. Dopf, H.M. Hertz, H. Brismar, M. Wiklund, Proliferation and viability of adherent cells manipulated by standing-wave ultrasound in a microfluidic chip, Ultrasound Med. Biol. 33 (2007) 145–151.
[79] R. ORorke, C. Wood, C. Walti, S. Evans, A. Davies, J. Cunningham, Acoustomicrofluidics: transporting microbubble and microparticle arrays in acoustic traps using surface acoustic waves, J. Appl. Phys. 111 (2012). 094911-1–094911-8.
[80] T. Laurell, F. Petersson, A. Nilsson, Chip integrated strategies for acoustic separation and manipulation of cells and particles, Chem. Soc. Rev. 36 (2007) 492–506.
[81] D.R. Gossett, W.M. Weaver, A.J. Mach, S.C. Hur, H.T.K. Tse, W. Lee, et al., Label-free cell separation and sorting in microfluidic systems, Anal. Bioanal. Chem. 397 (2010) 3249–3267.
[82] H. Bruus, Acoustofluidics 10: scaling laws in acoustophoresis, Lab Chip 12 (2012) 1578–1586.
[83] S. Kapishnikov, V. Kantsler, V. Steinberg, Continuous particle size separation and size sorting using ultrasound in a microchannel, J. Stat. Mech. Theory Exp. 2006 (2006). P01012.
[84] A. Lenshof, C. Magnusson, T. Laurell, Acoustofluidics 8: applications of acoustophoresis in continuous flow microsystems, Lab Chip 12 (2012) 1210–1223.
[85] W. Zhang, K. Kai, D.S. Choi, T. Iwamoto, Y.H. Nguyen, H. Wong, et al., Microfluidics separation reveals the stem-cell-like deformability of tumor-initiating cells, Proc. Natl. Acad. Sci. 109 (2012) 18707–18712.
[86] P. Preira, V. Grandné, J.M. Forel, S. Gabriele, M. Camara, O. Theodoly, Passive circulating cell sorting by deformability using a microfluidic gradual filter, Lab Chip (2013)

[87] J.A. Davis, D.W. Inglis, K.J. Morton, D.A. Lawrence, L.R. Huang, S.Y. Chou, et al., Deterministic hydrodynamics: taking blood apart, Proc. Natl. Acad. Sci. 103 (2006) 14779–14784.
[88] L.R. Huang, E.C. Cox, R.H. Austin, J.C. Sturm, Continuous particle separation through deterministic lateral displacement, Science 304 (2004) 987–990.
[89] S. Zheng, H. Lin, J.Q. Liu, M. Balic, R. Datar, R.J. Cote, et al., Membrane microfilter device for selective capture, electrolysis and genomic analysis of human circulating tumor cells, J. Chromatogr. A 1162 (2007) 154–161.
[90] H.K. Lin, S. Zheng, A.J. Williams, M. Balic, S. Groshen, H.I. Scher, et al., Portable filter-based microdevice for detection and characterization of circulating tumor cells, Clin. Cancer Res. 16 (2010) 5011–5018.
[91] M. Hosokawa, T. Hayata, Y. Fukuda, A. Arakaki, T. Yoshino, T. Tanaka, et al., Size-selective microcavity array for rapid and efficient detection of circulating tumor cells, Anal. Chem. 82 (2010) 6629–6635.
[92] R. Rosenberg, R. Gertler, J. Friederichs, K. Fuehrer, M. Dahm, R. Phelps, et al., Comparison of two density gradient centrifugation systems for the enrichment of disseminated tumor cells in blood, Cytometry 49 (2002) 150–158.
[93] M. Zourob, S. Elwary, A. Turner, Principles of Bacterial Detection: Biosensors, Recognition Receptors, and Microsystems, Springer, New York, 2008.
[94] F.A. Gomez, Biological Applications of Microfluidics, Wiley-Interscience, Hoboken, NJ, 2008.
[95] M.U. Kopp, A.J. de Mello, A. Manz, Chemical amplification: continuous-flow PCR on a chip, Science 280 (May 15 1998) 1046–1048.
[96] C. Zhang, D. Xing, Miniaturized PCR chips for nucleic acid amplification and analysis: latest advances and future trends, Nucleic Acids Res. 35 (2007) 4223–4237.
[97] Y. Xia, J.J. McClelland, R. Gupta, D. Qin, X.M. Zhao, et al., Replica molding using polymeric materials: a practical step towards nanomanufacturing, Adv. Mater. 9 (1997) 147–149.
[98] A.T. Woolley, D. Hadley, P. Landre, A.J. de Mello, R.A. Mathies, M.A. Northrup, Functional integration of PCR amplification and capillary electrophoresis in a microfabricated DNA analysis device, Anal. Chem. 68 (1996) 4081–4086.
[99] H. Nakano, K. Matsuda, M. Yohda, T. Nagamune, I. Endo, T. Yamane, High-speed polymerase chain-reaction in constant flow, Biosci. Biotechnol. Biochem. 58 (Feb 1994) 349–352.
[100] M. Elwenspoek, H.V. Jansen, Silicon micromachining, Cambridge University Press, Cambridge, England; New York, 1998.
[101] M. Piatak Jr., M. Saag, L. Yang, S. Clark, J. Kappes, K. Luk, et al., High levels of HIV-1 in plasma during all stages of infection determined by competitive PCR, Science 259 (1993) 1749.
[102] S.-H. Yeh, C.-Y. Tsai, J.-H. Kao, C.-J. Liu, T.-J. Kuo, M.-W. Lin, et al., Quantification and genotyping of hepatitis B virus in a single reaction by real-time PCR and melting curve analysis, J. Hepatol. 41 (2004) 659–666.
[103] J.M. Walboomers, M.V. Jacobs, M.M. Manos, F.X. Bosch, J.A. Kummer, K.V. Shah, et al., Human papillomavirus is a necessary cause of invasive cervical cancer worldwide, J. Pathol. 189 (1999) 12–19.
[104] T.C. Quinn, L. Welsh, A. Lentz, K. Crotchfelt, J. Zenilman, J. Newhall, et al., Diagnosis by AMPLICOR PCR of chlamydia trachomatis infection in urine samples from women

and men attending sexually transmitted disease clinics, J. Clin. Microbiol. 34 (1996) 1401–1406.
[105] H. Palmer, H. Mallinson, R. Wood, A. Herring, Evaluation of the specificities of five DNA amplification methods for the detection of *Neisseria gonorrhoeae*, J. Clin. Microbiol. 41 (2003) 835–837.
[106] M. Boeckh, M. Huang, J. Ferrenberg, T. Stevens-Ayers, L. Stensland, W.G. Nichols, et al., Optimization of quantitative detection of cytomegalovirus DNA in plasma by real-time PCR, J. Clin. Microbiol. 42 (2004) 1142–1148.
[107] K. Ohno, K. Tachikawa, A. Manz, Microfluidics: applications for analytical purposes in chemistry and biochemistry, Electrophoresis 29 (Nov 2008) 4443–4453.
[108] J. Khandurina, T.E. McKnight, S.C. Jacobson, L.C. Waters, R.S. Foote, J.M. Ramsey, Integrated system for rapid PCR-based DNA analysis in microfluidic devices, Anal. Chem. 72 (Jul 1 2000) 2995–3000.
[109] E.A. Ottesen, J.W. Hong, S.R. Quake, J.R. Leadbetter, Microfluidic digital PCR enables multigene analysis of individual environmental bacteria, Science 314 (Dec 1 2006) 1464–1467.
[110] R.H. Liu, J.N. Yang, R. Lenigk, J. Bonanno, P. Grodzinski, Self-contained, fully integrated biochip for sample preparation, polymerase chain reaction amplification, and DNA microarray detection, Anal. Chem. 76 (2004) 1824–1831.
[111] L.A. Legendre, J.M. Bienvenue, M.G. Roper, J.P. Ferrance, J.P. Landers, A simple, valveless microfluidic sample preparation device for extraction and amplification of DNA from nanoliter-volume samples, Anal. Chem. 78 (Mar 1 2006) 1444–1451.
[112] T. Nakayama, Y. Kurosawa, S. Furui, K. Kerman, M. Kobayashi, S.R. Rao, et al., Circumventing air bubbles in microfluidic systems and quantitative continuous-flow PCR applications, Anal. Bioanal. Chem. 386 (Nov 2006) 1327–1333.
[113] C.J. Easley, J.M. Karlinsey, J.M. Bienvenue, L.A. Legendre, M.G. Roper, S. H. Feldman, et al., A fully integrated microfluidic genetic analysis system with sample-in-answer-out capability, Proc. Natl. Acad. Sci. U. S. A. 103 (Dec 19 2006) 19272–19277.
[114] R.H. Liu, J. Bonanno, J. Yang, R. Lenigk, P. Grodzinski, Single-use, thermally actuated paraffin valves for microfluidic applications, Sens. Actuator B Chem. 98 (2004) 328–336.
[115] S. Haeberle, R. Zengerle, Microfluidic platforms for lab-on-a-chip applications, Lab Chip 7 (2007) 1094–1110.
[116] T. Thorsen, S.J. Maerkl, S.R. Quake, Microfluidic large-scale integration, Science 298 (2002) 580–584.
[117] S.L. Spurgeon, R.C. Jones, R. Ramakrishnan, High throughput gene expression measurement with real time PCR in a microfluidic dynamic array, PLoS One 3 (2008). e1662.
[118] N.B. Tsui, R.A. Kadir, K.A. Chan, C. Chi, G. Mellars, E.G. Tuddenham, et al., Noninvasive prenatal diagnosis of hemophilia by microfluidics digital PCR analysis of maternal plasma DNA, Blood 117 (2011) 3684–3691.
[119] T.K. Yung, K.A. Chan, T.S. Mok, J. Tong, K.-F. To, Y.D. Lo, Single-molecule detection of epidermal growth factor receptor mutations in plasma by microfluidics digital PCR in non-small cell lung cancer patients, Clin. Cancer Res. 15 (2009) 2076–2084.
[120] R.J. Lipshutz, S.P.A. Fodor, T.R. Gingeras, D.J. Lockhart, High density synthetic oligonucleotide arrays, Nat. Genet. 21 (Jan 1999) 20–24.

[121] D. Gresham, M.J. Dunham, D. Botstein, Comparing whole genomes using DNA microarrays, Nat. Rev. Genet. 9 (Apr 2008) 291–302.
[122] C.E. Massie, I.G. Mills, ChIPping away at gene regulation, EMBO Rep. 9 (Apr 2008) 337–343.
[123] A. Sassolas, B.D. Leca-Bouvier, L.J. Blum, DNA biosensors and microarrays, Chem. Rev. 108 (Jan 2008) 109–139.
[124] J. de Leon, M.T. Susce, E. Murray-Carmichael, The AmpliChip (TM) CYP450 genotyping test—integrating a new clinical tool, Mol. Diagn. Ther. 10 (2006) 135–151.
[125] S.J. Gardiner, E.J. Begg, Pharmacogenetics, drug-metabolizing enzymes, and clinical practice, Pharmacol. Rev. 58 (Sep 2006) 521–590.
[126] E.M. Southern, Detection of specific sequences among DNA fragments separated by gel electrophoresis, J. Mol. Biol. 98 (1975) 503–517.
[127] K. Weber, M. Osborn, The reliability of molecular weight determinations by dodecyl sulfate-polyacrylamide gel electrophoresis, J. Biol. Chem. 244 (1969) 4406–4412.
[128] C.S. Effenhauser, G.J. Bruin, A. Paulus, M. Ehrat, Integrated capillary electrophoresis on flexible silicone microdevices: analysis of DNA restriction fragments and detection of single DNA molecules on microchips, Anal. Chem. 69 (1997) 3451–3457.
[129] V. Dolnik, S. Liu, S. Jovanovich, Capillary electrophoresis on microchip, Electrophoresis 21 (2000) 41–54.
[130] Y. Cheng, W. Lin, Y. Yen, L. Chen, P. Hwu, Q. Liu, et al., Ratio quantification of gene dosage by Agilent 2100 Bioanalyzer for detection of somatic gene deletions, J. Biophys. Chem. 2 (2012).
[131] L.J. Hathaway, S. Brugger, A. Martynova, S. Aebi, K. Mühlemann, Use of the Agilent 2100 bioanalyzer for rapid and reproducible molecular typing of *Streptococcus pneumoniae*, J. Clin. Microbiol. 45 (2007) 803–809.
[132] C.Y. Lu, D.J. Tso, T. Yang, Y.J. Jong, Y.H. Wei, Detection of DNA mutations associated with mitochondrial diseases by Agilent 2100 bioanalyzer, Clin. Chim. Acta 318 (2002) 97–105.
[133] F. Sanger, S. Nicklen, A.R. Coulson, DNA sequencing with chain-terminating inhibitors, Proc. Natl. Acad. Sci. 74 (1977) 5463–5467.
[134] J. Shendure, H. Ji, Next-generation DNA sequencing, Nat. Biotechnol. 26 (2008) 1135–1145.
[135] B.M. Paegel, R.G. Blazej, R.A. Mathies, Microfluidic devices for DNA sequencing: sample preparation and electrophoretic analysis, Curr. Opin. Biotechnol. 14 (2003) 42–50.
[136] R.G. Blazej, P. Kumaresan, R.A. Mathies, Microfabricated bioprocessor for integrated nanoliter-scale Sanger DNA sequencing, Proc. Natl. Acad. Sci. 103 (2006) 7240–7245.
[137] D. Branton, D.W. Deamer, A. Marziali, H. Bayley, S.A. Benner, T. Butler, et al., The potential and challenges of nanopore sequencing, Nat. Biotechnol. 26 (2008) 1146–1153.
[138] J.J. Kasianowicz, E. Brandin, D. Branton, D.W. Deamer, Characterization of individual polynucleotide molecules using a membrane channel, Proc. Natl. Acad. Sci. 93 (1996) 13770–13773.
[139] M. Jain, S. Koren, K.H. Miga, J. Quick, A.C. Rand, T.A. Sasani, et al., Nanopore sequencing and assembly of a human genome with ultra-long reads, Nat. Biotechnol. (2018).

[140] M. Wanunu, T. Dadosh, V. Ray, J. Jin, L. McReynolds, M. Drndić, Rapid electronic detection of probe-specific microRNAs using thin nanopore sensors, Nat. Nanotechnol. 5 (2010) 807.
[141] E.A. Manrao, I.M. Derrington, A.H. Laszlo, K.W. Langford, M.K. Hopper, N. Gillgren, et al., Reading DNA at single-nucleotide resolution with a mutant MspA nanopore and phi29 DNA polymerase, Nat. Biotechnol. 30 (2012) 349–353.
[142] Z. Liu, Y. Wang, T. Deng, Q. Chen, Solid-state nanopore-based DNA sequencing technology, J. Nanomater. 2016 (2016).